Pd bonded on Nb(001): Dependence of noble metal and ferromagnetic characteristics on film thickness

E. Hüger[1,2] and K. Osuch[3,4,*]

[1]*Institute of Physics and Physical Technology, Technical University Clausthal, D-38678 Clausthal-Zellerfeld, Germany*

[2]*Department of Biomaterials, Institute for Bioprocessing and Analytical Measurement Techniques, Rosenhof, D-37308 Heilbad Heiligenstadt, Germany*

[3]*Department of Physics, University of South Africa, P.O. Box 392, 0003 Pretoria, South Africa*

[4]*Faculty of Physics, Warsaw University of Technology, Koszykowa 75, 00-662 Warszawa, Poland*

(Received 29 March 2005; revised manuscript received 24 June 2005; published 15 August 2005)

Experimental observations confirmed by density functional theory (DFT) calculations show that strong epitaxial bonds between Pd atoms and the substrate can induce two competing properties: nobleness and ferromagnetic order in the same material, i.e., Pd bonded on Nb(100). Angle-resolved ultraviolet photoelectron spectroscopy measurements, confirmed by first principles, self-consistent DFT calculations show that the strong, direct bonds between a Pd monolayer and Nb(001) push the *d*-band center of the monolayer toward lower binding energies, which results in the Pd reactivity comparable to that of the noble metal Ag. The strong epitaxial constraint of the Nb(001) substrate induces a $(11\bar{2}0)$-oriented hexagonal close-packed structure in thicker Pd films. First principles, self-consistent DFT calculations with spin-orbit coupling included performed at 0 K show that Pd in this structure is ferromagnetically ordered at the optimum lattice constant. Its bands at the Fermi level are flatter in comparison to those of Pd in its natural, nonmagnetic, face-centered-cubic structure, leading to the density of states (DOS) at the Fermi level which fulfills the Stoner criterion for ferromagnetism. We identify these bands in the bulk band structure and probe them with angle-resolved ultraviolet photoelectron spectroscopy in $(11\bar{2}0)$-oriented hexagonal close-packed Pd films.

DOI: 10.1103/PhysRevB.72.085432 PACS number(s): 68.43.Fg, 73.20.At, 75.50.Cc, 82.80.Pv

I. INTRODUCTION

Ferromagnetic order and nobleness are two sought for but, at the same time, competing properties of metals. Noble metals are characterized by filled valence *d* bands situated well below the Fermi level, which result in their poor surface reactivity and ability to resist corrosion against reactive gases like H_2, O_2, N_2, CO and the dissolution of these gases in their bulk. In contrast, holes in the valence *d* bands of a metal are needed for a preferential spin alignment to occur. Much work has been done so far to obtain a metal characterized by these two competing properties. As a candidate for such a metal we chose Pd because of its interesting electronic structure, in the atomic state it has fully occupied *d* states like the noble metals Cu, Ag, and Au whereas in the bulk phase its *d* states are not occupied, making Pd a reactive metal, that is often used in catalysis.[1] On the other hand, as soon as Pd atoms are involved in bonds, holes are created in the valence *d* bands. The electronic structure of metallic Pd is characterized by a high density of states (DOS) at the Fermi energy $[N(E_F)]$ which is on the threshold of fulfilling the Stoner criterion for ferromagnetism.[2–4] The Stoner criterion for ferromagnetism,[2] $IN(E_F)>1$, where *I* is the Stoner parameter and $N(E_F)$ is the density of states at the Fermi level of the paramagnetic state, tests whether the potential energy gain through the exchange interaction by establishing ferromagnetic spin alignment overcomes the energy cost of the rearrangement of the band occupancy. Since the Stoner parameter *I*, which is related to exchange interaction, is only insignificantly influenced by different crystal symmetries, the decisive role in establishing ferromagnetic order is played by the density of states at the Fermi energy. This is especially the case for 4*d* and 5*d* metals, where the Stoner parameter shows practically no dependence on the atomic number.

In this work we show that both properties, i.e., ferromagnetic order and noble-metal-like character, can be induced in Pd by altering its electronic structure through change of the bonding angle or the strength of the bonds between atoms. Beside scientific interest there is also technological interest in inducing in Pd a ferromagnetic state or an electronic structure similar to that of a noble metal. Ferromagnetic order is well known to provide useful engineering and technological applications.[5–13] In particular, with the information revolution and the ever growing need to acquire, store, and retrieve information, the science and technologies attached to magnetic recording have experienced explosive growth. Central to those pursuits is the material science of magnetism as it applies to surfaces, interfaces, and thin films.[5–13]

Of technological interest is also a Pd surface with a noble-metal-like character, especially an open one, like that formed by one monolayer (ML) of Pd bonded on Nb(001). Due to its noble-metal-like character (which will be shown further on), it can be kept free from contamination. One very promising area of application of such a surface can be by the use of fullerenes.[14,15] In this context, the pseudomorphic (ps)[16] Pd ML on Nb(001) can play a twofold role, its metallic character will very probably lead to a layer-by-layer growth of the deposited fullerenes and its nobleness will successfully prevent the decomposition of fullerenes making their complete removal from the surface possible, without contaminating the sample with carbon.[15]

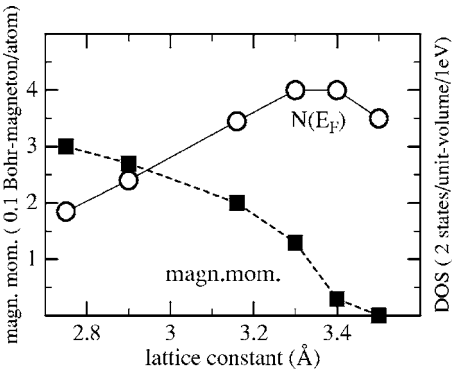

FIG. 1. Magnetic moment (marked with squares) and DOS at the Fermi level (marked with circles) of a free standing Pd(001) monolayer as a function of the lattice constant.

Curiously enough, all the attempts thus far to obtain Pd with both properties consisted in weakening the bonds between Pd atoms. The bond weakening, which could be achieved through lattice dilation or electron localization associated with a reduced coordination number, lead to more states with antibonding character generated at the Fermi level. As a result,[17] an increase of $N(E_F)$ could be achieved large enough to fulfill the Stoner criterion for ferromagnetism.[3,4] At the same time, the weakening of the interaction between Pd atoms, made their electronic structure more atomiclike, with the d states completely filled.[18] This interplay between ferromagnetic order and the filling of the d states by expanding the Pd lattice can be seen in Fig. 1, where the magnetic moment and the DOS at the Fermi level are presented of a free standing Pd(001) ML as a function of the lattice constant.

A free standing Pd ML with the periodicity of the (001) plane of the fcc-Pd lattice is ferromagnetically ordered because it corresponds to a bulk lattice which is strongly expanded in the [100] direction (see Sec. II C). The expansion of the bulk lattice reduces the interaction between the atoms thus reducing the d-band width, which is a measure of the interaction strength. The narrowing of the d-band width increases the DOS sufficiently enough to fulfill the Stoner criterion for ferromagnetism. A further increase of the lattice constant of the ML results in an increase of the DOS at the Fermi level, which should further strengthen the ferromagnetic order. On the contrary, the magnetic moment decreases with further lattice expansion as shown in Fig. 1. This happens because the lattice expansion increases the occupancy of the d bands of the Pd ML and, consequently, the electronic structure of Pd becomes atomiclike. As a result, the number of electrons available for spin anisotropy and, consequently, the magnetic moment is reduced (Fig. 1). Now, the deposition of metals on suitable substrates can enlarge, via pseudomorphism,[16,19] the in-plane lattice constant of a film. This does not lead, however, to an enlarged atomic volume, because in the direction perpendicular to the surface, the film relaxes, reducing its out-of-plane lattice constant in such a way, that the atomic volume is conserved (equal to that of the natural phase). So, it becomes clear that the weakening of the bonds between Pd atoms can neither make a noble metal of Pd nor induce ferromagnetic order in it. In this work we show that an opposite route, which consists in creating stronger bonds should be followed to induce both noble-metal properties and ferromagnetism in Pd. This can be done by depositing Pd on Nb(001).[20–32] Experimental data confirmed by first-principle calculations demonstrates that the strong bonds between Pd and Nb(001) induce (i) a noble-metal-like electronic structure in Pd atoms which are in direct contact with Nb atoms and (ii) the hexagonal close-packed phase in thicker Pd films which orders ferromagnetically at the optimum lattice constant. The paper is organized as follows. Section II describes the experimental and theoretical procedure used. In Sec. III we present and discuss our experimental and theoretical results. Section IV summarizes our results.

II. EXPERIMENTAL AND COMPUTATIONAL DETAILS

A. Measurement equipment

The experiments were performed in a VG-ESCA-LAB MKII spectrometer [(ESCA) electron spectroscopy for chemical analysis], which was connected with a home-built chamber equipped with a reflection high-energy electron diffraction (RHEED) apparatus. The RHEED chamber was pumped by a titanium sublimation pump with a liquid nitrogen (LN_2) cooled wall and via the main (ESCA) system by a LN_2-baffled diffusion pump which produced the base pressure of 3×10^{-11} mbar after the system had been backed at ~500 K for 24 hours. The base pressure of the chamber (3×10^{-11} mbar) rose to 7×10^{-11} mbar during the metal deposition from preoutgased evaporators situated in the both chambers. The home-built water-cooled metal evaporators allowed deposition rates of 0.03–10 ML per minute. The sample was mounted on an home-built, exchangeable specimen cartridge which was inserted into a manipulator with translation and rotation degrees of freedom. Heating with electron bombardment was used to reach temperatures as high as the metallic melting point, cooling with liquid nitrogen to lower it to 150 K. The temperature was measured with a W-3%Re/W-25%Re thermoelement which was calibrated at high temperatures with a disappearing filament pyrometer. The sample could be rapidly transferred in ultrahigh vacuum (UHV) between the two subsystems within 8 minutes, which made it possible to correlate the deposition rates determined by RHEED and by the electron spectroscopy.[33,34] RHEED was not only used to determine the substrate and layer structure, orientation and morphology but also the growth rate via specular beam intensity oscillations. A 20 keV beam with an emission current of 9 μA was used at grazing angles of incidence ~0.3°, which made RHEED very sensitive to the surface morphology. The ESCA chamber contained a hemispherical analyzer with the resolution of 60 meV at the pass energy of 2 eV, a monochromatized x-ray source set to the Al K_α line (1486.6 eV), an electron gun for Auger electron spectroscopy (AES) which was operated at the emission current of 1–3 μA and the beam energy of 1.8 keV. Unpolarized and polarized vacuum ultraviolet light from a Leybold capillary noble-gas resonance discharge lamp with the photon energies of 21.22 eV (He I) and 16.85 eV (Ne I) was used in the ultraviolet photoelectron spectroscopy (UPS) measurements. For AES and x-ray photoelectron spectroscopy (XPS)

the angular acceptance of the analyzer was set to ±12°, for x-ray photoelectron diffraction (XPD) and angle-resolved UPS (ARUPS) to ±1°. The surface quality and growth mode was examined with RHEED, AES, and ARUPS. The geometric structure was determined with RHEED and XPD, the electronic structure with AES, XPS, and ARUPS. The chemical composition of the sample was checked mainly with AES. A quadrupole mass spectrometer was used to determine the gas composition and the stability of the evaporators. A VG-Microtech EX05 ion source whose beam could be deflected, scanned, and focused on the sample, was used for sputtering.

B. Nb(001) substrate cleaning

The substrate used in this work was a single crystal of Nb ($6\times10\times0.5$ mm^3), which was mirrorlike polished and oriented to within 0.04° of the (001) face. The orientation was checked with x-ray Laue photographs. The stress of the crystal was minimized by supporting it on a preoutgased W disk and by the use of Ta sheet springs.

The removal of oxygen from Nb and Ta surfaces without serious deterioration of the surface perfection has been a major problem in nearly all studies of these surfaces in the past.[35] The difficulty of removing oxygen is due to the high solubility and diffusivity of O in these metals and the low vapor pressure of its suboxides. The solubility of O in Nb has a maximum of 6 atomic percent at about 2050 K. It decreases above this temperature in the absence of oxygen sources due to desorption in the form of NbO and NbO_2. However, at partial pressures above 10^{-11} mbar Nb, absorbs oxygen.[36] As a result, an equilibrium concentration of O in bulk Nb occurs that acts as an oxygen contamination source for the surface upon cooling a Nb crystal.

In the past, only outgassing of very thin Nb samples, such as thin polycrystalline Nb foils, in UHV close to or even above the melting point (2700 K), was successful in cleaning the bulk sufficiently enough for only negligible oxygen segregation to occur upon cooling. Unfortunately, during the cooling great parts of the Nb surface crystallize in the dense-packed (110) structure, and not in the desired (001) orientation. Single crystals distort badly during such extreme treatments. When they are outgased at lower temperatures, their surfaces still show oxygen contamination upon cooling.[37] The (001) face is particularly difficult to clean. Occasional reports of oxygen-free (001) surfaces based on UPS studies of the surfaces heated for long times at very high temperatures,[38] contain no information on the surface perfection. Other structurally sensitive studies indicate that the surfaces became rather imperfect during this treatment.[35] Heating in hydrogen and sputtering has not been successful either.[35]

For epitaxy and other studies it is important to prepare well-ordered surfaces with bulk lateral periodicity which remain free of oxygen upon heating after sputter cleaning at low temperatures. On the Nb(001) surface, however, oxygen induces a rearrangement of the surface Nb atoms, destroying its bulk lateral periodicity.[37,39–41] We have found an experimental procedure which suppresses oxygen diffusion to the Nb surface while maintaining the bulk lateral periodicity of Nb(001).[41] This was achieved by depositing suitable metals, like Pd or Au, on Nb(001) after its low sputter cleaning, followed by annealing to elevated temperatures (1200 K to 1600 K). This process lead to a flat, (1×1) Nb(001)-like surface terminated with 1 ps ML of Pd or Au, with the needed bulk lateral periodicity of the (001)-oriented Nb crystal, which we used as the substrate for our metal epitaxy investigations.[41,42]

C. Calculation procedure

The calculations were performed within the framework of density functional theory (DFT), using the full potential augmented plane wave (FLAPW) method and the local spin density approximation (LSDA)[43,44] as implemented in the WIEN2K package.[45] First scalar relativistic calculations were carried out and subsequently spin-orbit coupling was included in a second variation step.[45] 142 k points were used in the irreducible wedge of the Brillouin zone (IBZ). The adsorption systems and the Nb_3Pd_1 bulk alloy were simulated with a slab model, which is known to be very efficient and precise for various surface problems.[46]

Figure 2 presents the unit cells used in the slab calculations. The unit cell of the slab was for the free standing Pd ML and for the Pd ML on Nb(001), a tetragon with the height equal to that of 18 nonrelaxed Nb(001) MLs (18×1.65 Å), whose base was the two-dimensional unit cell of the Nb(001) layer. The unit cell of Pd absorbed on Nb(001) contained nine Nb(001) ML covered by a ps ML of Pd, followed by the free space of 8 ML [see Fig. 2(b)]. The vacuum for a free standing Pd(001) ML was 17 ML thick [see Fig. 2(a)]. The unit cell of the Nb_3Pd_1 bulk alloy was four Nb(001) ML thick, as a Pd ML was followed there by three Nb ML without empty space in between [see Fig. 2(a)]. For these systems, the lattice constant in the lateral planes was set to the experimental value of the Nb(001) substrate ($a_{Nb}=3.30$ Å), while the vertical positions of the surface and of the first four subsurface layers were optimized through atomic force calculations (z relaxation), i.e., the derivatives of the total energy with respect to the atomic positions were minimized. In addition, the in-plane lattice constant of the free standing Pd(001) monolayers was varied as shown in Fig. 1.

The bulk calculations were performed at 560 k points in the irreducible wedge of the Brillouin zone (IBZ). The optimum lattice constant of Pd was determined by minimizing the total energy as a function of the lattice constant. Convergence of the self-consistent calculations was assumed when the electron charge distance defined as $\int|\rho_n(r)-\rho_{n-1}(r)|d^3r$, where ρ is the electron charge density and n is the iteration number, was smaller than $1\times10^{-4}e$ in three consecutive iterations. It should be mentioned that LDA (LSDA) underestimates the lattice constants of transition metals.[47] Gradient corrections, on the other hand, dramatically reduce the error[47–49] and also give the correct natural phase stability,[50–52] but they tend to overestimate the magnetic moment.[47,53,54]

III. RESULTS AND DISCUSSION

The electronic structure of a Pd layer adsorbed on Nb(001) and monitored in situ with UPS is shown in Fig. 3

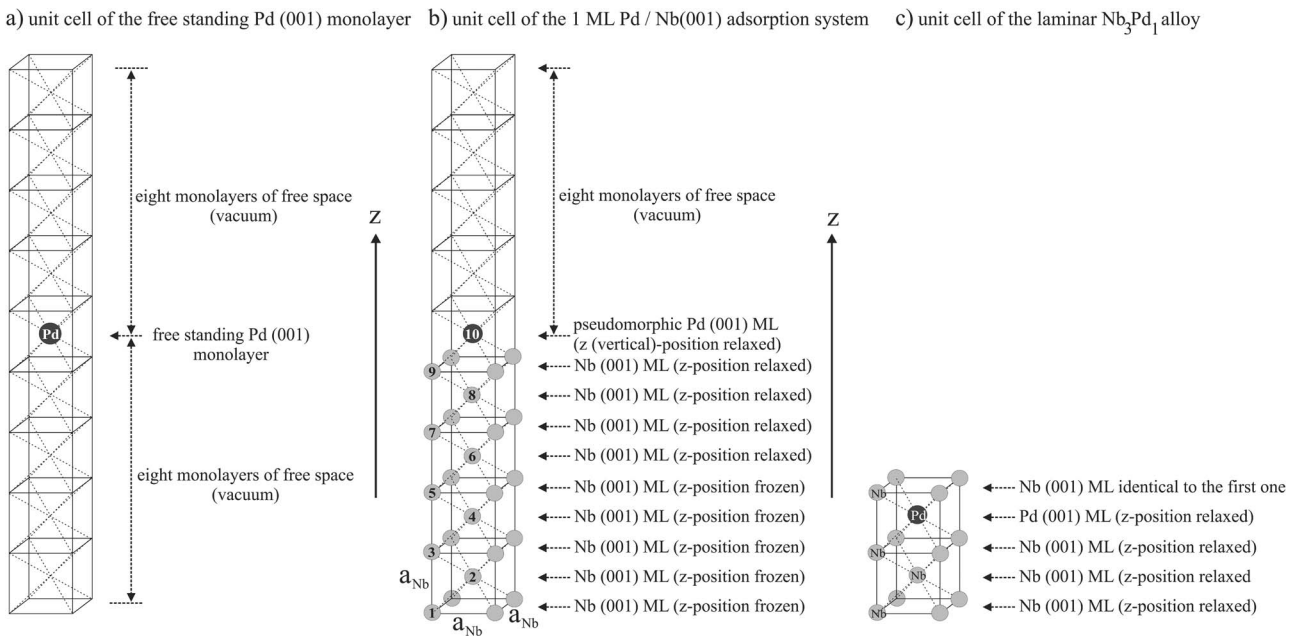

FIG. 2. Schematic representation of the unit cells used in the slab calculations. All the unit cells are tetragons. (a) Unit cell of the free standing Pd(001) monolayer. The height of the tetragonal unit cell is equal to that of 18 nonrelaxed Nb(001) ML (18×1.65 Å). The vacuum between two consecutive monolayers is 17 nonrelaxed Nb(001) ML thick. The in-plane lattice constant of the free standing Pd(001) monolayers was varied as shown in Fig. 1. (b) Unit cell of the 1 ML Pd/Nb(001) system. It contains nine Nb(001) ML followed by a ML of Pd and of the free space of 8 ML. The height of the unit cell is equal to that of 18 nonrelaxed Nb(001) ML (18×1.65 Å). The lattice constant in the lateral planes was set to the experimental value of the Nb(001) substrate ($a_{\mathrm{Nb}}=3.30$ Å), while the vertical positions of the surface and of the first four subsurface layers were optimized through atomic force calculations (z relaxation), i.e., the derivatives of the total energy with respect to the atomic positions were minimized. (c) Unit cell of the laminar Nb_3Pd_1 bulk alloy. Three Nb(001) monolayers are followed by a Pd(001) monolayer in a bcc structure. Hence, all Pd atoms have eight nearest neighbors, all of them being Nb atoms. The height of the unit cell is equal to that of four nonrelaxed Nb(001) ML (4×1.65 Å). The lattice constant in the lateral planes was set to the experimental value of the Nb(001) substrate ($a_{\mathrm{Nb}}=3.30$ Å). The vertical positions of all atoms were optimized through atomic force calculations (z relaxation).

as a function of the layer thickness given in ML.

It is identical to that of Pd deposited on W(001).[33] For Pd, unusual UPS emissions appear for 1 ML and also for thicker Pd films. 1 ML of Pd adsorbed on Nb(001) exhibits energetically deep lying emissions like the noble-metal Cu,[55] whereas thicker Pd films display only a strong UPS peak just below the Fermi level like the ferromagnetic metals Ni (Ref. 56) and Co.[33,57–60] The aim of this work is to determine the properties of the Pd layers exhibiting the unusual UPS emissions, i.e., of 1 ML Pd deposited on Nb(001) and of thick Pd films grown on this substrate. To this end their geometric and electronic structure will be determined using electron diffraction and electron spectroscopy measurements. The experimental results will be compared with *ab initio* DFT calculations.

A. 1 ML Pd

1. Electronic structure and bonding

RHEED shows a (1×1) diffraction pattern until 2 ML of Pd have been deposited on the Nb(001) substrate, indicating a pseudomorphic growth of the Pd layer over this thickness range, similarly to the growth of Pd on W(001).[33] However, in contrast to a ps ML of Pd on W(001), a ML of Pd on Nb(001) gives sharp and intense RHEED (1×1) patterns, showing very good long-range order. The latter ML is expanded by 44% in comparison to the bulk Pd(001) surface, which gives the atomic next-nearest-neighbor distance $a_{\mathrm{Nb}}=3.30$ Å. So, the Pd atoms are forced to be positioned in lateral Nb(001) sites. This indicates that strong bonds must have been established between Pd and Nb, which are able to counteract the increase of the total energy due to the large expansion of the ps ML of Pd. These strong bonds manifest themselves in the existence of long-range order evident from the sharp and intense UPS emissions obtained from the Pd ML on Nb(001) [Figs. 3 and 4(a)].

Figure 4 compares the UPS emissions from 1 ML Pd on Nb(001) with those obtained from a (111)-oriented bulk-Cu sample. 1 ML of Pd on Nb(001) shows UPS emissions located well below the Fermi energy, similar to those obtained from Cu [Fig. 4(b)]. These energetically deep lying UPS peaks, unusual for Pd, do not appear exclusively in normal emission, as it is shown in Fig. 5.

It can be assumed that the UPS peaks in Fig. 5 mainly consists of emissions from the ps Pd ML on Nb(001), because the photoionization cross section of Pd is for He I excitation (21.22 eV) three times larger than that of Nb,[61] and the photoelectrons He I excited from Nb valence states have in Nb(001) the escape depth of less than 3 ML.[62] Since the Pd ML does not have translational symmetry perpendicularly to the surface, its electronic structure is given by the $E(k_{\parallel})$

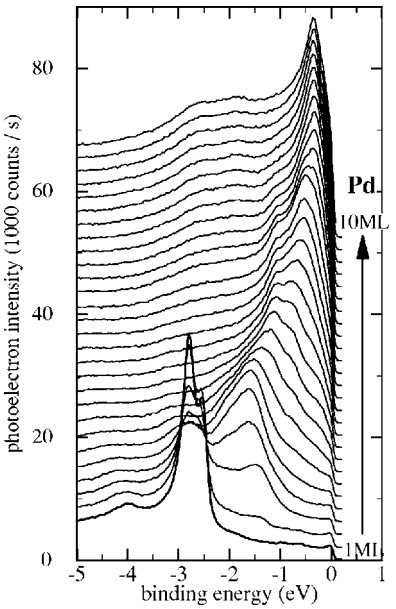

FIG. 3. Normal emission He I-UPS spectra taken *in situ* during the growth of Pd on Nb(001) at 150 K.

band dispersion, which can be determined from the angular dependence of the UPS emissions.

The $k_{\|}$ component (parallel to the film surface) of the wave vector is conserved in photoelectron emission.[55] Thus, the $k_{\|}$ values of the initial emission states can be calculated from $k_{\|}=1/\hbar\sqrt{2m_eE_{\mathrm{kin}}}\sin\theta=1/\hbar\sqrt{2m_e(h\nu-\Phi-|E_B|)}\sin\theta$, where θ is the emission angle, E_{kin}, the kinetic energy of an emitted photoelectron; Φ, the work function of the film; E_B, the binding energy of the initial state; and $h\nu$ is the energy of an absorbed photon.[55] The resulting $E(k_{\|})$ dependence for the ML of Pd on Nb(001) is presented in Fig. 6(a).

The circle size gives an estimate of the intensity of the UPS emission coming from the corresponding state, big circles correspond to high and small circles to low UPS emissions. It can be observed that the Pd ML on Nb(001) exhibits strong emissions from states lying at deep binding energies.

DFT calculations were performed to help us understand why the Pd ML on Nb(001) shows energetically deep lying states like those of the noble metal Cu [Figs. 4(a) and 4(b)].

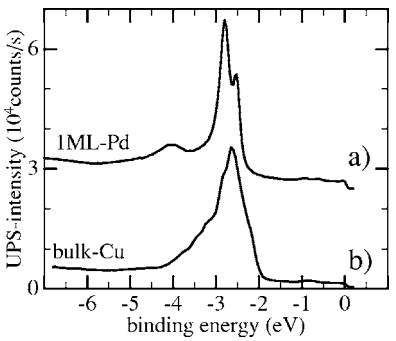

FIG. 4. Normal emission He I-UPS spectra of a Pd monolayer bonded to Nb(001) [curve marked with (a)] and of a (111)-oriented fcc Cu [curve marked with (b)].

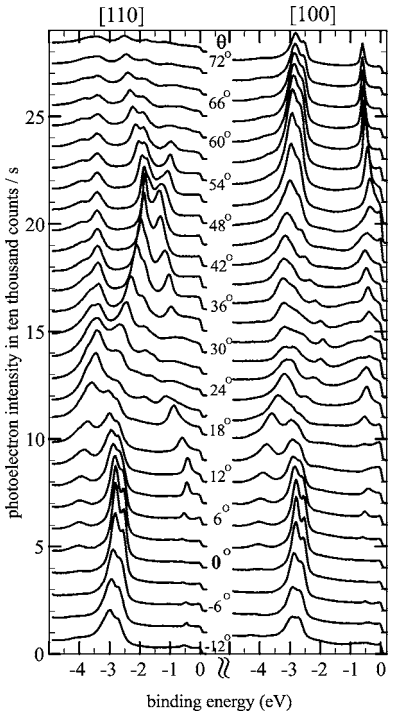

FIG. 5. ARUPS spectra of a Pd ML bonded to Nb(001). The emission angle was changed in the high symmetry directions $[110]_{\mathrm{Nb}}$ and $[100]_{\mathrm{Nb}}$, which were determined with RHEED.

They show that if the surface Nb layer of the Nb(001) substrate is replaced by a Pd ML, strong attractive forces act on the Pd atoms, trying to reduce the distance between the Pd ML and the Nb(001) surface. These strong forces are indicative of strong bonds established between Pd and Nb. The forces are minimized only when the distance between the Pd ML and the first subsurface Nb ML is reduced by 23%, that between the two subsequent Nb ML is expanded by 1.8% and the following one contracted by 1.2%. Only after the full z relaxation does the calculated electronic structure of the Pd ML on Nb(001) [Fig. 6(b)] coincide with the measured one [Fig. 6(a)]. The good agreement between the experimentally and theoretically determined band structures also confirms our conclusion, obtained on the grounds of RHEED measurements, that the first ML of Pd bonds pseudomorphically to Nb(001).

Note also good agreement between the angle integrated UPS (Fig. 7) and the DOS of the z-relaxed ps Pd ML on Nb(001) [Fig. 8(c)], which falls in with the good coincidence of the experimentally and theoretically determined geometric and electronic structures of Pd on Nb(001).

Figure 8 shows how different is the DOS of Pd bonded on Nb(001) [Fig. 8(c)] in comparison to that of the free standing Pd ML [Fig. 8(a)] and of bulk Pd [Fig. 8(b)]. The bonding to Nb shifts a great part of the Pd states of the free standing Pd ML to lower binding energies. As a result, the DOS of the Pd ML on Nb(001) [Fig. 8(c)] has more states lying at deep binding energies than bulk Pd [Fig. 8(b)].

Bonding is easily visualized with charge density maps. The cuts through the charge density difference of the relaxed (1 ML Pd)/Nb(001) presented in Fig. 9 display an agglomeration of charge between Pd and subsurface Nb atoms,

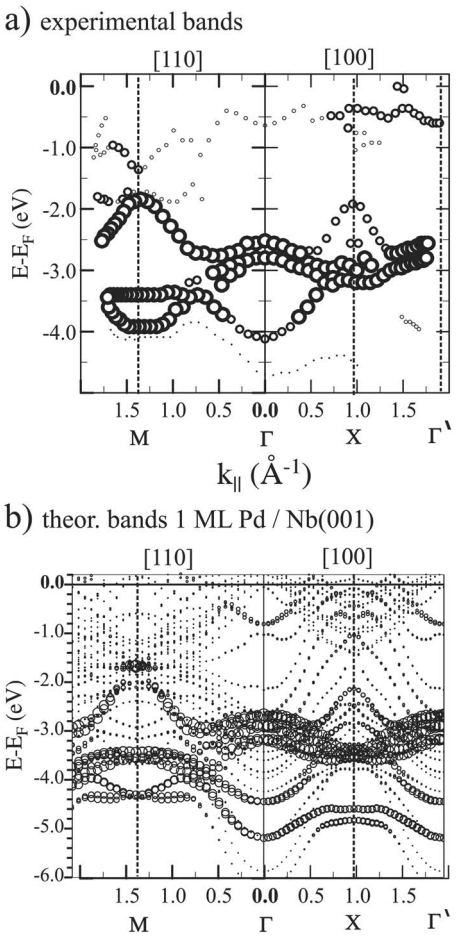

FIG. 6. (a) $E(k_{\|})$ bands obtained from the ARUPS measurements presented in Fig. 5. The circle size gives an indication of the UPS intensity, big (small) circles correspond to high (low) UPS emissions. (b) Bands of a pseudomorphic ML of Pd on Nb(001) obtained from DFT calculations of the z-relaxed structure. The Pd ML relaxed towards the Nb surface. The equilibrium distance between the Pd monolayer and the Nb(001) surface layer is by 22.3% smaller than the bulk distance between Nb(001) monolayers. The relaxation of the following (Nb) layers is +1.8%, −1.2%, +1.8%, and −4.3%, respectively. The circle size gives the contribution of the Pd states to the band states of the 1 Pd ML on Nb(001).

which is responsible for strong bonding between Pd and Nb, resulting in energetically low lying Pd states.[32,46,63]

Our experiments and calculations indicate that the shifts of Pd states to deep lying energies occur due to the bonding between Nb and Pd and not because of the Pd atoms (situated on the surface) having a lower coordination number than in the bulk. Figure 10(a) shows that if the (1 ML Pd)/Nb(001) sample is covered with Ag, the energy positions of the Pd states do not change. This means that the strength of the bonds between Pd and Nb is not influenced by the covering with Ag. Further, if Pd bonds to more Nb atoms, as in Nb_3Pd_1, where the Pd atoms are fully coordinated (they have the maximum number of nearest-neighbor Nb atoms), even more Pd states are pushed to deeper lying energies [compare Figs. 8(c) and 8(d)].

The shifting of the Pd d states to lower lying energies depends on the ratio (q) between the number of the nearest-neighbor Nb atoms which bond to a Pd atom and the number of Pd atoms involved in these bonds. A Pd ML bonded to Nb(001) has $q=1$, whereas the Pd ML in between Nb ML of the Nb_3Pd_1 alloy has $q=2$. Submonolayer Pd coverages on the Nb(001) surface have $q=1$ for Pd inside two-dimensional (2D) islands and $q=2$ (or $q=3$) for Pd atoms situated on the peripheries of these islands, whereas isolated Pd atoms bonded to Nb(001) have $q=4$. Our calculations and measurements demonstrate that the larger the q, the more of the Pd d states shift to deeper binding energies. This is exemplified by Figs. 8 and 11. Figures 8(c) and 8(d) show that in the case of the layered Nb_3Pd_1 alloy the bonding of a Pd ML inside the Nb bulk ($q=2$) pushes more Pd d states to lower energies than for 1 ML of Pd bonded to Nb(001) ($q=1$). Indeed,

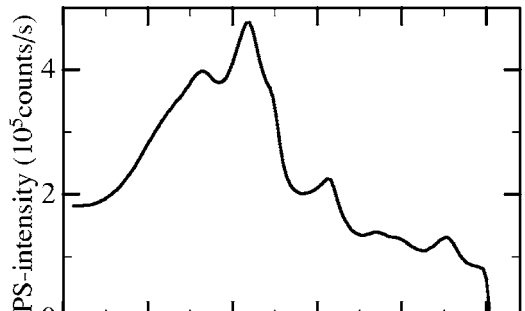

FIG. 7. Approximation of the angle integrated UPS obtained through the sum of all the ARUPS spectra of the ps Pd ML deposited on Nb(001), collected in the high symmetry directions ([110] and [100]). These spectra are to be compared with the calculated density of d-states shown in Fig. 8(c). Note good coincidence of the experimental (this figure), and theoretical results [Fig. 8(c)].

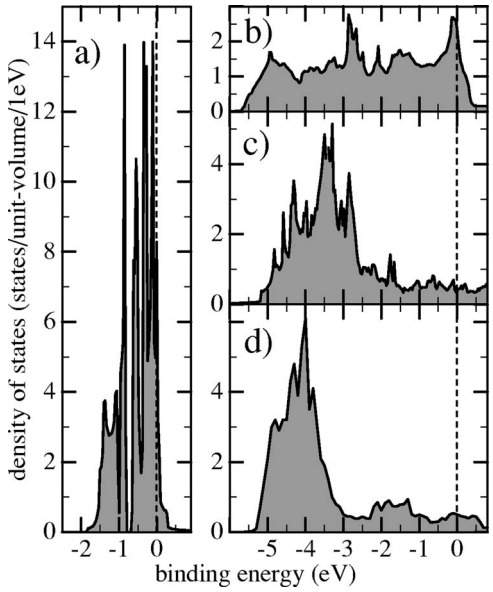

FIG. 8. Calculated paramagnetic d-projected local density of states of Pd in (a) a free standing Pd(001) ML with the lattice constant $a=3.30$ Å. (b) Bulk fcc Pd. (c) z-relaxed ps Pd ML bonded to Nb(001). (d) Nb_3Pd_1 bulk alloy.

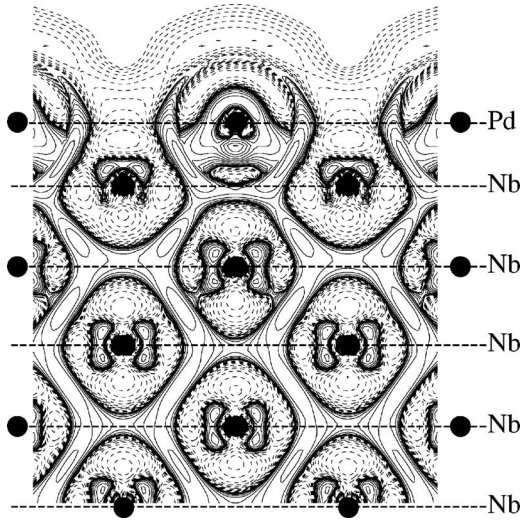

FIG. 9. Maps of the difference between the superposed charge densities of the constituent atoms and the self-consistent charge density of the z-relaxed Pd ML bonded on Nb(001). Solid (dashed) lines indicate charge density accumulation (depletion). The cross sections are along the {110} planes (of Nb). The horizontal dashed lines indicate the z positions of the ML. The positions of atomic nuclei are given by black circles. The observed charge rearrangement is in response to the bonding between Pd and Nb (Ref. 32).

ARUP spectra of the Pd-Nb bulk alloy display Pd emissions shifted by ~0.3 eV towards lower energies relative to those of (1 ML Pd)/Nb(001).[41] This is in agreement with the situation in Pd alloys, where low-lying Pd states are also obtained in the case when the nearest-neighbors of Pd are atoms of *sp* metals like Mg (Ref. 64) and Al (Ref. 65) or metals with a low *d*-band occupancy like V,[65–67] Ta,[65] Zr,[68,69] Sc, Ti, Y, La, Ce, Pr, Nd, Sm, Th, Ur.[65]

Figures 10(d)–10(f) refer to a submonolayer of Pd deposited on a sputter-rough Nb(001) surface. The low deposition temperature (150 K) and especially the strong Pd-Nb bond cause a low mobility of the Pd atoms on the surface. This low diffusivity should lead for submonolayer coverages (e.g., 0.2 ML) to Pd aggregated in small 2D islands or even to isolated Pd atoms bonded to Nb(001). Thus, for low coverages, the fraction of Pd atoms with $q=2,3,4$ should be larger than for coverages larger than 0.5 ML. Figure 10(d) shows that low sub-ML Pd coverages (0.2 ML) on Nb(001), where large fractions of Pd atoms have $q=2$, $q=3$ or even $q=4$, exhibit Pd-UPS emissions centered at −3.5 eV. These emissions are shifted to energies by 0.4 eV and 0.7 eV lower than those of Pd in bulk Nb ($q=2$) and of 1 ML Pd on Nb(001) ($q=1$), respectively. If the sub-ML coverage increases, the number of Pd atoms positioned inside the 2D islands ($q=1$) also increases relative to that of Pd atoms at the island edges, leading, in comparison to 0.2 ML of Pd, to additional UPS emissions [Figs. 10(e) and 10(f)] which are characteristic of 1 ML Pd bonded to Nb(001).

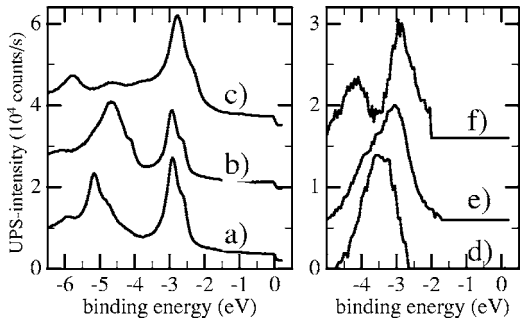

FIG. 10. Normal emission He I-UPS spectra from (a), (b), (c) (1 ML Pd)/Nb(001) covered with (a) 1 ML Ag; (b) 2 ML Ag; and (c) 1 ML Au. (d), (e), (f) Difference of normal emission UPS spectra between (d) (0.2 ML Pd)/Nb(001) and Nb(001); (e) (0.6 ML Pd)/Nb(001) and Nb(001); (f) (0.6 ML Pd)/Nb(001) and (0.2 ML Pd)/Nb(001). The deposition was done at 150 K. In (d), (e), (f) Pd was deposited on a lightly sputtered, clean Nb(001) surface.

2. Reactivity

Hammer and Norskov[70] showed that the reactivity of a *d*-band metal can be predicted on the grounds of the shape of its *d*-valence density of states. They pointed out, that the factors which determine the nobleness of metals, in terms of poor surface reactivity and of ability to resist corrosion in reactive gases like H_2, O_2, N_2, CO and the dissolution of these gases in their bulk, are (i) the energy position of the *d*-band center; (ii) the degree of *d*-band filling; (iii) the coupling matrix element; (iv) the strength of the *d*-*d* bonds (the cohesive energy). An increase in the occupancy of the *d* states and the lowering of the energy position of the *d* band center increase the occupancy of the reactive gas—metal states and hence are a measure of the reactivity reduction of a metal surface. The reactivity also decreases with the increasing coupling-matrix element.[70] The coupling matrix element between the substrate and adsorbate, is determined by the bond geometry [e.g., by the bond lengths and the extension of the *d* states (which in fact also determines the bond lengths)]. For a given bond geometry, the valence band width is a measure of the coupling matrix element.[71] On the other hand, the strength of the *d*-*d* bonds (the cohesive energy) is a measure of the susceptibility of metal bonds to being broken up (as a result, stable compounds such as hibrides, oxides, and carbides are created).[70] Thus, the reactivity (i.e., the nobleness) of a *d*-band metal depends on the form of its valence *d* band. This paves the way to the atomic engineering of materials with desired catalytic activity and selectivity.

The calculated value of 9.50 of the *d*-band filling of the Pd ML bonded to Nb(001) is slightly larger than that of bulk Pd (9.29), whereas the *d*-band widths of the two systems are the same [Figs. 8(b) and 8(c)]. In contrast, the key factor determining the reactivity, i.e., the position of the *d*-band center,[70] shows larger differences in the two cases. The *d*-band centers of bulk Nb, bulk Pd and a free standing Pd(001) ML with the lattice constant of 3.30 Å lie at $\varepsilon_d = +1.4$ eV, $\varepsilon_d = -1.8$ eV [for the (001)-surface layer of fcc Pd (Ref. 72)] and $\varepsilon_d = -0.5$ eV, respectively. On the other hand, the bonding of the Pd ML to Nb(001) pushes its *d*-band center to $\varepsilon_d = -2.7$ eV, i.e., to an energy which is smaller than that of bulk Pd ($\varepsilon_d = -1.8$ eV) and even slightly smaller than that of the noble metal Cu ($\epsilon_d = -2.6$ eV).[70] The coupling matrix element of Pd is smaller than that of Au, but

larger than that of Cu and, in fact, even larger than that of Ag.[70] So, due to the deeper-lying *d*-band center and a similar *d*-band width, it should be expected that the ML of Pd bonded to Nb(001) is less reactive than bulk Cu.

Reactivity measurements show that Pd ML bonded to W, Nb(110), and Ta(110) have a reactivity comparable to that of the noble metal Ag.[63] In our case, the Pd ML is by 35% less densely packed than Pd bonded to Nb(110) or Ta(110). The ARUPS spectra of the Pd ML on Nb(001) contain UPS emissions from Pd states lying at much lower binding energies than those of Pd on Nb(110) or Ta(110).[63] Pan *et al.*[26] showed, using self-consistent DFT calculations, that the Pd-Nb binding energy for Pd/Nb(001) is more than twice larger than for Pd/Nb(110). Thus, the origin of the larger shifts of Pd states to lower energies for Pd on Nb(001) lies in the stronger bonding of Pd to the more open Nb(001) surface than to the denser-packed Nb(110) surface. We can, therefore, argue that the reactivity of the lattice-expanded ML of Pd bonded to Nb(001) is at least the same, if not lower, than that of Pd bonded on Nb(110) or Ta(110), which is comparable to the reactivity of the noble metal Ag.

The substrate used in this work, i.e., Nb(001), is characterized by strong oxygen segregation from the bulk toward the surface and also by a strong reactivity towards contamination with CO and H_2 from the residual gas existing in ultrahigh vacuum. Consequently, a cleaned Nb(001) surface left in UHV for 30 minutes at 300 K shows in AES and ARUPS substantial C and O contamination. In contrast, the Pd ML bonded to Nb(001) saturates the surface in such a manner that it stops the oxygen segregation from the Nb bulk towards the surface. We observed that, even if the Pd ML on Nb(001) was left in UHV for more than 30 hours, no contamination of the surface by the residual gas could be detected with AES and UPS. This leads to the conclusion that the bonding of the two reactive metals Pd and Nb leads to a Pd terminated surface, which exhibits properties of a noble metal.

B. Thick Pd films deposited on Nb(001)

In contrast to the deposition of Au and Ag on the (1 ML Pd)/Nb(001) substrate [Figs. 10(a)–10(c)], further deposition of Pd on this substrate shifts the UPS emission closer to the Fermi level (Fig. 3). The UPS emission of 2 ML Pd bonded to Nb(001) occurs at −1.75 eV, similarly to that of 1 ML Pd bonded to W(110).[73] However, further deposition of Pd on Nb(001) leads to UPS emissions which are different from those of Pd on W(110). Pd films thicker than 4 ML[73] deposited on W(110) show UPS emissions centered at the binding energies of −1.2 eV and −2.4 eV, which are characteristic of the He I-UPS emission from (111)-oriented Pd samples.[74] In these samples the hexagonal close packed (111) planes of Pd are parallel to the substrate surface, i.e., parallel to the densest packed (110) planes of the (110)-oriented W substrate. In contrast, the ARUPS spectra obtained from thick Pd films bonded to Nb(001) (see Fig. 3) show a single strong peak close to the Fermi level, similar to that obtained from Ni films deposited on Fe(001).[56] Furthermore, the diffraction pattern of Pd on Nb(001) is also similar to that of Ni on Fe(001).[75,76]

In Sec. III B 1 we will determine the crystal structure of thick Pd films deposited on Nb(001) which produce the strong UPS emission near the Fermi level. We will show that the growth of Pd on the open (001) surface of Nb exhibits similarities but also differences to the growth of Pd on the closest-packed (110) surface of Nb. The two processes are similar since in both cases [i.e., in the epitaxy of Pd on (110)- or (001)-oriented W or Nb substrates] the hexagonal close-packed planes of Pd grow parallel to the close-packed planes of W or Nb. The differences are related to the different orientations of the substrates, i.e., the (110) or (001) orientation. Pd grows on the (110)-oriented Nb or W substrates, with its hexagonal close-packed (111) atomic planes parallel to the substrate surface.[73] The stacking sequence axis of the hexagonal close-packed Pd layers is then perpendicular to the surface. In this direction (i.e., the surface normal direction) the substrate (i.e., Nb) does not influence directly the crystal structure of the adsorbate (i.e., that of Pd). Consequently, there is no epitaxy-based constraint for the Pd films grown on Nb(011) or on W(011), which would result in a change of its natural stacking sequence. In the case of Nb(001) [or W(001)], Pd also grows with its hexagonal close-packed atomic planes parallel to the densest packed (110) plane of Nb (or W). But now the hexagonal close-packed atomic planes of Pd lie perpendicularly to the surface, because the (110) planes of Nb (or W) are perpendicular to the Nb(001) [or W(001)] substrate. Consequently, the stacking sequence axis lies parallel to the Nb(001) [or W(001)] surface where the substrate has a direct influence on the crystal structure of the growing epitaxial films. We will show that the epitaxial constraint of the Nb(001) surface induces in the Pd film a hexagonal stacking sequence instead of its natural fcc stacking. In Secs. III B 2, III B 3, III B 4, and III B 5 we will determine the electronic structure of the Pd films deposited on Nb(001). We will also show there that the stacking sequence of the hexagonal close-packed Pd planes, which is induced by the arrangement of the Nb(001) surface, is responsible for the strong peak in UPS close to the Fermi level (Fig. 3).

1. Film structure

Figure 11(a) shows a RHEED transmission pattern obtained from thick Pd films deposited on Nb(001). It is identical to that observed in Ni on Fe(001).[75]

Centered patterns were also observed in LEED studies of Ni films on Fe(001) (Ref. 76) and in RHEED studies of Ni and Cu films on Fe(001) and on Au(001).[75] The origin of these patterns was for a long time unknown.[77] Wang *et al.*[76] tried to explain the patterns as produced by a strained (001)-oriented, body centered tetragonal structure. However, such a structure would give rise to a noncentered diffraction pattern rather than to the centered pattern of Fig. 11. In a previous short paper[77] on the interrelation between the fourfold symmetry of (001)-oriented cubic substrates and the magnetic properties of films grown on them, we mentioned in passing that the centered RHEED pattern obtained from those films originates from an hcp stacking sequence of the adsorbate.

To find this hypothetical structure, we applied x-ray photoelectron diffraction (XPD), which gives information about the local atomic environment in real space. XPD[78–80] makes

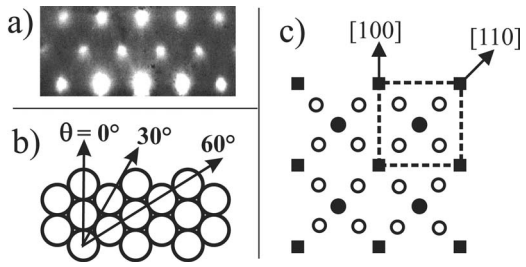

FIG. 11. (a) RHEED transmission pattern obtained from a 20 ML thick Pd film deposited on Nb(001). The incident beam was along the [110] direction of the Nb(001) surface. (b) Sketch of the fcc(111) plane for the explanation of the XPD measurements. (c) The reciprocal lattice observed in a RHEED reflection from flat surfaces of Pd deposited on Nb(001) as would be seen by LEED, the projection of the reciprocal rods on the surface plane. The black squares form the (1×1) reciprocal structure of the pseudomorphic surface. The squares together with the black filled circles form the centered $c(2\times2)[p(\sqrt{2}\times\sqrt{2})R45°]$ (surface) reciprocal lattice. If supplemented with the nonfilled circles, they form the $p(2\sqrt{2}\times\sqrt{2})R45°\oplus p(\sqrt{2}\times2\sqrt{2})R45°$ reciprocal lattice. The unit cell of the (1×1) structure is sketched with dashed lines.

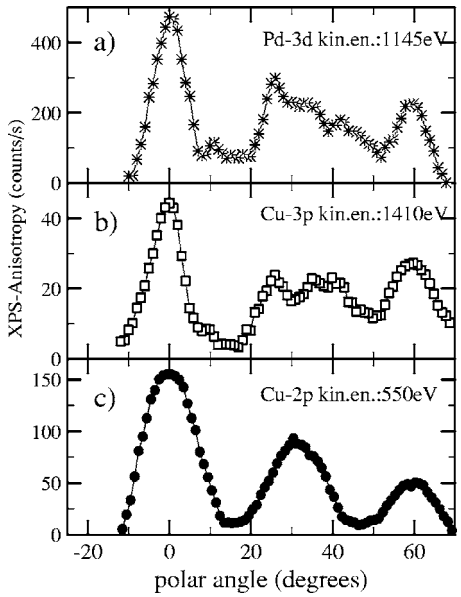

FIG. 12. Emission-angle distribution of the background corrected x-ray photoelectron intensity from (a) the Pd-3*d* core levels of a 16 ML thick Pd film deposited on Nb(001); (b), (c) the Cu-3*p*- [panel (b)] and Cu-2*p*-core levels [panel (c)] of a 16 ML thick Cu film deposited on Nb(001). The polar angle was changed in the plane perpendicular to the surface and aligned with the high symmetry $[110]_{Nb}$ direction. The surface normal direction corresponds to $\theta=0°$. The kinetic energy of the Pd-3*d*, Cu-3*p*, and Cu -2*p* photoelectrons excited by the Al-$K\alpha(h\nu=1486.6$ eV) radiation was ~1145 eV, 1410 eV, and 550 eV, respectively. For background correction, the angle distribution was measured of inelastic electrons with the kinetic energy of 1050 eV for Pd, 1300 eV for 3*p* -Cu, and 450 eV for 2*p*-Cu. This background emission, which did not exhibit any peaks, was then multiplied by a constant factor and subtracted from the elastic signal.

use of the forward-focusing effect displayed by fast (with the kinetic energy over 300 eV) photoelectrons moving along atomic rows on their way toward the surface. The forward focusing produces a modulation in the angle dependence of the photoelectron intensity which corresponds to the angle position of the densest packed atomic chains. The faster the electrons and the denser the atomic rows, the stronger the corresponding intensity modulation.

Figure 12(a) shows the polar-angle dependence of the XPS signal emitted from the 3*d* core levels of Pd along the high symmetry direction $[110]_{Nb}$, in which the RHEED pattern of Fig. 11(a) was obtained. The polar-angle distribution of the 3*p*-core levels of Cu in thin Cu films deposited on Nb(001) [Fig. 12(b)] also displays the same centered RHEED pattern as Pd on Nb(001) (Fig. 11) or Ni on Fe(001).[75]

The comparison of the XPD curve of Fig. 12(b) (obtained with photoelectrons having the kinetic energy of 1410 eV) with that of Fig. 12(c) [obtained from the same Cu film with slower photoelectrons emitted from the Cu-2*p* levels ($E_{kin}=550$ eV)] shows that only the angle positions of the peaks situated between $\theta=20°$ and $\theta=43°$ change. This is an indication, that the peaks situated at $\theta=0°$ and $\theta\sim60°$ come from the forward focusing along dense packed atomic chains, whereas the peaks around $\theta=30°$ consist of, beside the contribution from the forward focusing along atomic rows, second-order interference effects. Thus, it can be concluded that perpendicularly to the surface and along the $[110]_{Nb}$ direction there are atomic planes of Pd (Cu) with sixfold symmetry, i.e., hexagonal close-packed (111) planes [see Fig. 11(b)]. The XPD results demonstrate that these planes and the densest-packed direction ([110]) lie perpendicularly to the surface. Therefore, it can be inferred that the orientation of the Pd films on Nb(001) is $(110)_{Pd}$, $\langle211\rangle_{Pd}\|(001)_{Nb}$, $\langle110\rangle_{Nb}$. In this orientation, the stacking (111) planes are perpendicular to the surface, whereas the stacking sequence axis [111] is parallel to it, pointing along the $[110]_{Nb}$ direction.

Indeed, the XPD pattern of (Fig. 12) is similar to that obtained from a (110)-oriented, single Cu crystal along the $\langle211\rangle$ azimuth (curve $\phi=55°$ in Fig. 5 of Ref. 81). However, the XPD curves presented in Fig. 12 are also similar to those obtained from $(11\bar{2}0)$ thick hcp Co films.[82] This happens because the peaks in the XPD curves presented in Fig. 12 are dominated by the forward focusing along the densest-packed atomic chains lying within the hexagonal close-packed planes [Fig. 11(b)]. Consequently, it is not possible to determine the stacking sequence of the hexagonal close-packed atomic planes of Pd deposited on Nb(001) on the grounds of the XPD results only. Let us see whether some light on the stacking sequence problem can be shed by the observed, centered RHEED pattern. To this end we will construct the expected RHEED-transmission patterns for the stacking sequence with the periodicity of two stacking planes (*d*-hcp structure), three stacking planes (fcc structure) and four stacking planes (*d*-hcp structure).

For a comparison of the expected RHEED patterns it is convenient to introduce nonconventional unit cells with the (110) planes as the basis planes. Figure 13 shows the (110)-

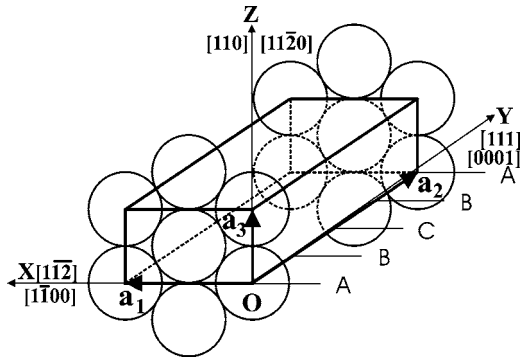

FIG. 13. The orthorhombic (110)-based unit cell spanned by the vectors $\mathbf{a_1}$, $\mathbf{a_2}$, $\mathbf{a_3}$ which are aligned with the axes of the Cartesian coordinate system and determined by the atomic periodicity in the [110], [111] ([0001]), and $\langle 211\rangle$([1$\bar{1}$00]) lattice directions, respectively.

based orthorhombic unit cell, delimited in the *OXZ* plane by densest-packed hexagonal atomic planes.

The (110)-based unit cell is spanned by the vectors $\mathbf{a_1}=a\sqrt{3}\mathbf{e_1}$, $\mathbf{a_2}=c\mathbf{e_2}$, and $\mathbf{a_3}=a\mathbf{e_3}$, where $\mathbf{e_1}$, $\mathbf{e_2}$, $\mathbf{e_3}$ are the unit vectors of the Cartesian coordinate system, a is the atomic nearest-neighbor distance in a fcc film, and c is the periodicity of the stacking planes in the stacking sequence direction ([111] for an fcc stacking and [0001] for a non-fcc stacking). The reciprocal lattices constructed from these unit cells are presented in Figs. 14, 15, and 16 for the stacking periodicity of two, three, and four stacking planes, respectively.

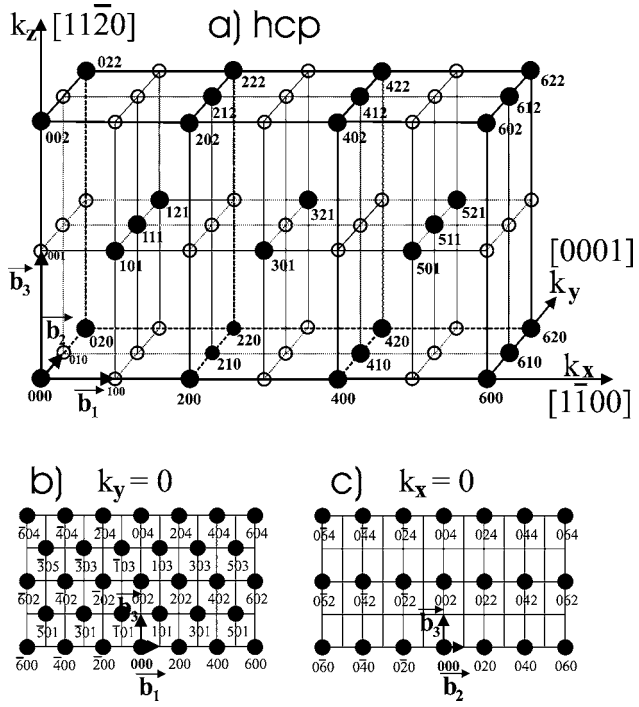

FIG. 14. (a) Reciprocal lattice of the hcp stacking sequence constructed from the orthorhombic (110)-based unit cell given in Fig. 13. Due to the structure factor (which influences the intensity of diffracted beams), the arrangement of the atoms inside the unit cell leads to systematic extinction of all the spots which correspond to the lattice points marked with nonfilled circles. The lattice points which lead to diffraction spots are marked with black filled circles. (b), (c) (0001) (b) and (1$\bar{1}$00) (c) sections correspond to the ($k_y=0$) and ($k_x=0$) planes, respectively. Only those lattice points which lead to diffraction spots are drawn. The scale in (b), (c) is four times smaller than in (a). The lines, formed by the reciprocal vectors $\mathbf{b_1}$, $\mathbf{b_2}$, $\mathbf{b_3}$, are only guides for the eyes.

The reciprocal orthorhombic unit cells are spanned by vectors $\mathbf{b_1}$, $\mathbf{b_2}$, $\mathbf{b_3}$, with $\mathbf{b_1}=[2\pi/(a\sqrt{3})]\mathbf{k_x}$, $\mathbf{b_2}=(2\pi/c)\mathbf{k_y}$, and $\mathbf{b_3}=(2\pi/a)\mathbf{k_z}$, where $\mathbf{k_x}$, $\mathbf{k_y}$, $\mathbf{k_z}$ are the unit vectors of the Cartesian coordinate system with $\mathbf{k_x}\|\mathbf{e_1}$, $\mathbf{k_y}\|\mathbf{e_2}$, and $\mathbf{k_z}\|\mathbf{e_3}$. Up to now, we have not considered the atomic arrangement inside the unit cell. The positions of the atoms inside the unit cell lead to systematic extinction of spots corresponding to the nonfilled circles. Because of the large extension of the Ewald sphere, RHEED transmission patterns correspond to plane cuts through the reciprocal structure lying perpendicularly to the primary beam. In contrast to the (001) substrate surface, which has fourfold symmetry, the $(110)_{\text{film}}$ and $(11\bar{2}0)_{\text{film}}$ surface has only twofold symmetry. Although the orthogonal [110] and [1$\bar{1}$0] directions of the (001)-oriented bcc-substrate surface are equivalent, the orthogonal directions $[0001]_{\text{film}}$ and $[1\bar{1}00]_{\text{film}}$ or $[111]_{\text{film}}$ and $[1\bar{1}\bar{2}]_{\text{film}}$ are not. Therefore, the adsorbate grows on the (001)-oriented cubic substrate in two orthogonal domains. One with $[0001]_{\text{film}}\|[110]_{\text{bcc-substrate}}$ and $[1\bar{1}00]_{\text{film}}\|[1\bar{1}0]_{\text{bcc-substrate}}$ and the other with $[0001]_{\text{film}}\|[1\bar{1}0]_{\text{bcc-substrate}}$ and $[1\bar{1}00]_{\text{film}}\|[110]_{\text{bcc-substrate}}$ for a non-fcc stacking. For the fcc stacking sequence of the adsorbate, one domain has $[111]_{\text{film}}\|[110]_{\text{bcc-substrate}}$

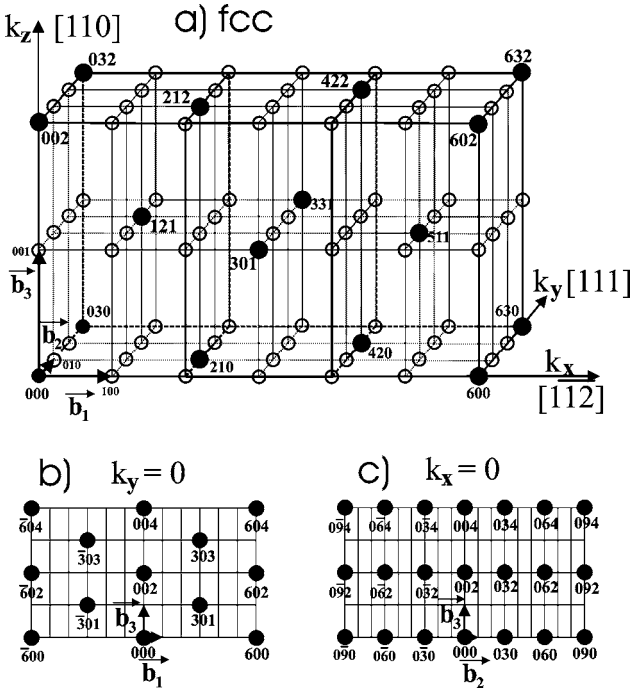

FIG. 15. The same as in Fig. 14, but now for the fcc-stacking sequence. Note that all the lattice points whose structure factors do not lead to a systematic extinction of diffraction spots (all black filled points) form the bcc lattice which is the reciprocal lattice of the fcc crystal.

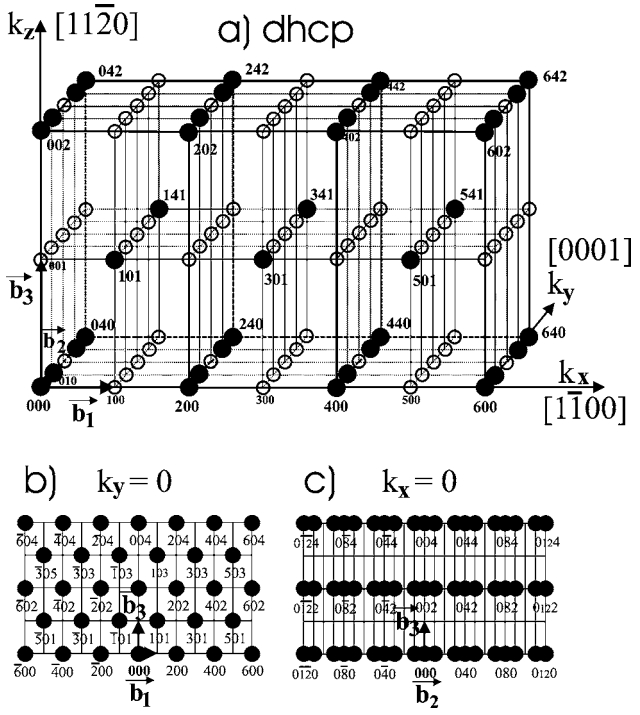

FIG. 16. The same as in Fig. 14, but now for the *d*hcp-stacking sequence (*ABCBA*). Note, that lattice points become more numerous in the stacking sequence direction (along $\mathbf{b}_2$).

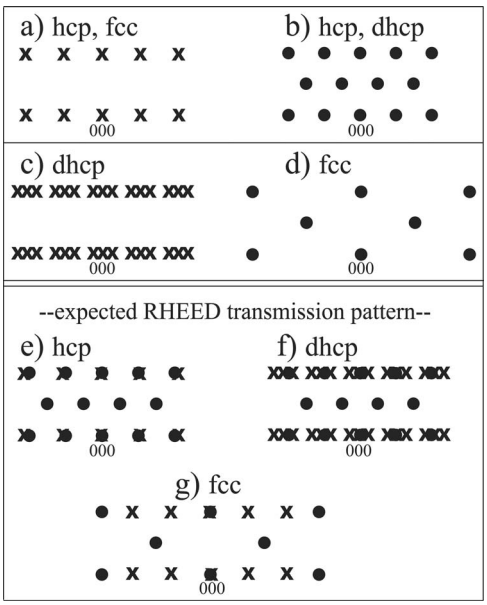

FIG. 17. (a) (1$\bar{1}$00) plane cut through the reciprocal structure of the hcp lattice which is identical to the (1$\bar{1}\bar{2}$) plane cut through the reciprocal structure of the fcc lattice. (b) (0001) plane cut through the reciprocal structure of the hcp and *d*hcp lattice. (c) (1$\bar{1}$00) plane cut through the reciprocal structure of the *d*hcp lattice. (d) (111) plane cut through the reciprocal structure of the fcc lattice. (e) The expected RHEED-transmission pattern of an hcp-stacking sequence is a superposition of panels (a) and (b). (f) The expected RHEED pattern of the *d*hcp-stacking sequence is a superposition of panels (c) and (b). (g) The expected RHEED pattern of the fcc-stacking sequence is a superposition of panels (a) and (d).

and $[1\bar{1}\bar{2}]_{\text{film}} \| [1\bar{1}0]_{\text{bcc-substrate}}$ and the other $[111]_{\text{film}} \| [1\bar{1}0]_{\text{bcc-substrate}}$ and $[1\bar{1}\bar{2}]_{\text{film}} \| [110]_{\text{bcc-substrates}}$. Thus, the RHEED transmission pattern observed in the diagonal ⟨110⟩ direction of the (001)-oriented bcc-substrate surface represents a superposition of plane cuts through the reciprocal lattice lying perpendicularly to the [0001] and [1$\bar{1}$00] directions for non-fcc stacking planes and to the $[111]_{\text{film}}$ and $[1\bar{1}\bar{2}]_{\text{film}}$ directions for the fcc stacking sequence. Therefore, the expected RHEED patterns must be superpositions of the $k_y=0$ and $k_x=0$ planes of Figs. 14, 15, and 16 and are presented in Figs. 17(e), 17(f), and 17(g) for the hcp-, *d*hcp-, and fcc-stacking sequence, respectively.

They clearly show that the RHEED transmission pattern [Fig. 11(a)], comes from the hcp stacking sequence [Fig. 17(e)]. The *d*-hcp stacking sequence shows an additional fourfold periodicity [Fig. 17(f)] which was occasionally seen in thick Pd films deposited on Nb(001) and in thick Pd films grown on W(001) (see Fig. 10 in Ref. 33).

The orientation relationship of (110)-oriented Pd on Nb(001) (sketched in Fig. 18) explains why the Pd films adopt the hexagonal stacking sequence.

For all stacking sequences, the hexagonal densest packed Pd planes lie perpendicularly to the Nb(001) surface and along its ⟨110⟩ direction [Fig. 18(b)]. The fcc-stacking sequence would place the stacking planes of Pd in much more unfavorable, in the case of metal bonding, adsorption sites, situated away from the hollow sites of the Nb(001) surface [Fig. 18(c)], than the hexagonal stacking sequences [Figs. 18(e) and 18(g)]. Panels (d), (f), (h) of this figure show the fit of the stacking sequence periodicity of Pd to the [110] direction of the Nb(001) surface. It is clear from panel (d) that the fcc-stacking sequence periodicity puts every second stacking plane of Pd in the most unfavorable on-top adsorption position. That stacking plane [sketched in the middle of panel (d)] will be forced by the epitaxial stress energy to move to one of the two hollow-site positions marked with arrows in Fig. 18(d), creating in this way an hcp [Fig. 18(f)] or *d*hcp [Fig. 18(h)] stacking sequence. Thus, the most favorable adsorption sites (the hollow sites) of the Nb(001) surface (which are arranged in a square geometry) force Pd to grow on it in a hexagonal stacking sequence.

A hexagonal stacking sequence also explains the centered $c(2\times2)$ and $(2\sqrt{2}\times\sqrt{2})R45^\circ \oplus (\sqrt{2}\times2\sqrt{2})R45^\circ$ reciprocal surface structures [see panel (c) of Fig. 11] observed, for example, for Pd and Cu on Nb(001) and on W(001) (Ref. 33) and for Ni on Fe(001).[76] The unit cell of the (11.0) surface of the hcp stacking, is $2\sqrt{2}\times\sqrt{2}$ times larger than, and rotated by $R45^\circ$ relative to that of the Nb(001) surface. Due to the fact that the hcp orientation grows on the square substrate in two domains, one with [0001] parallel to $[110]_{\text{Nb}}$, and the other with [1$\bar{1}$00] parallel to $[110]_{\text{Nb}}$, all the observed spots of the $c(2\times2)=(\sqrt{2}\times\sqrt{2})R45^\circ$ and $(2\sqrt{2}\times\sqrt{2})R45^\circ \oplus (\sqrt{2}\times2\sqrt{2})R45^\circ$ reciprocal surface structures are produced by the hcp- and *d*hcp-stacking sequences, respectively.

We have observed,[83] in addition, that if the Nb(001) adsorption sites are occupied by impurities like sulfur or saturated by oxygen, no hexagonal close packed sequence can be induced in Pd. We also showed[83] that *S* passivates Nb to such

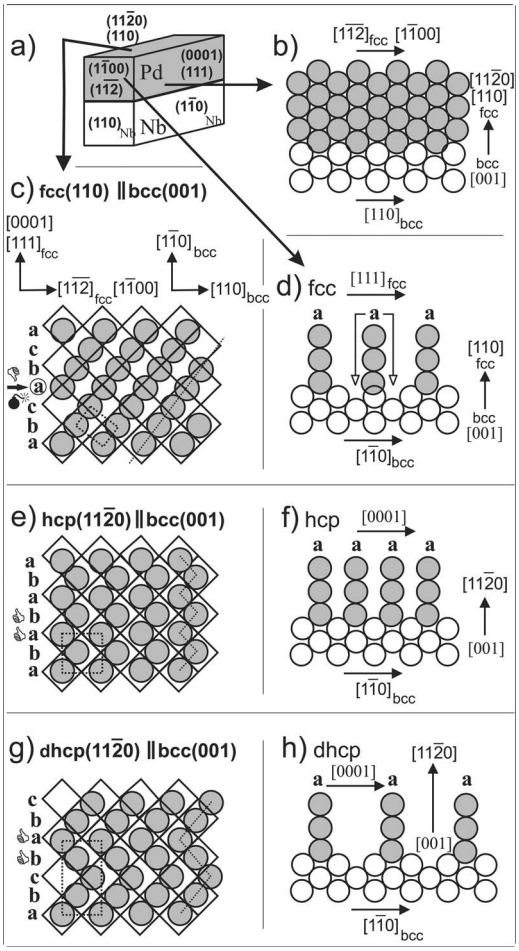

FIG. 18. (a) Orientation relationship of (110)-oriented Pd on Nb(001). For the fcc-stacking sequence [(a), (b), (c), (d)] the epitaxial relations are Pd(110)⟨211⟩‖Nb(001)⟨110⟩. For the hcp-[(a), (b), (e), (f)] and *d*hcp-[(a), (b), (g), (h)] stacking sequences the epitaxial relationship is Pd(11$\bar{2}$0)⟨1$\bar{1}$00⟩‖Nb(001)⟨110⟩. Panels (c), (e), (g) show the fit of the (110) plane of Pd for fcc- (c), hcp- (e), and *d*hcp- (g) stacking sequences to the (001) surface of the substrate. Pd atoms are represented by gray circles and Nb atoms are situated at the corners of the sketched quadratic (001) lattice. Panels (b), (d), (f), (h) show planar cuts perpendicular to the surface and along the $\langle 110\rangle_{\mathrm{Nb}}$ directions of the substrate. The substrate atoms are drawn here with nonfilled circles. (d), (f), (h) are along the stacking sequence axis.

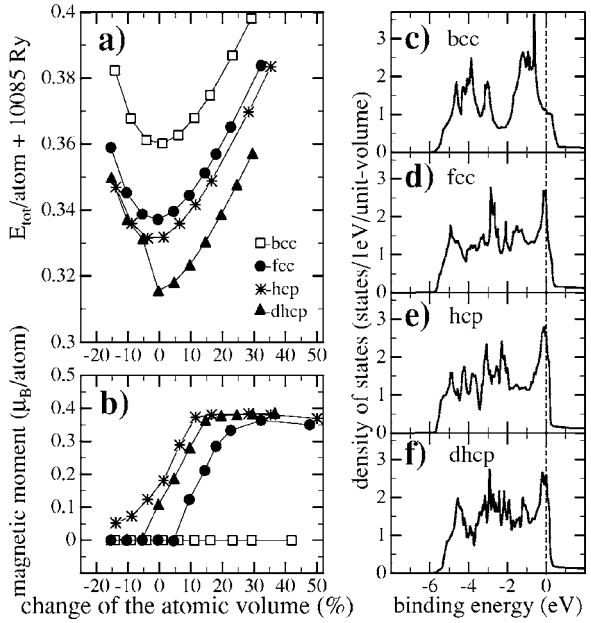

FIG. 19. (a), (b) Total energy (a) and magnetic moment (b) of bulk Pd in the bcc (squares), fcc (circles), hcp (stars), and *d*hcp (triangles) structure as a function of atomic volume expansion (+) or contraction (−) obtained from DFT spin-polarized calculations with spin-orbit coupling included. (c), (d), (e), (f) *d*-projected DOS of bulk Pd in the bcc (c), fcc (d), hcp (e), and *d*hcp structure (f) at the optimum lattice constant obtained from DFT non-spin-polarized calculations with spin-orbit coupling included.

an extent that Pd is only weakly bonded to a S (1×1)-terminated Nb(001) surface, growing nonepitaxially on it. Thus, the hcp and *d*hcp phase of Pd films deposited on Nb(001) occurs due to the strong bonding of Pd to Nb. Let us now see what properties the hcp and *d*hcp phases of Pd have.

2. Magnetism of Pd

In a recent paper[84] we have discussed the interrelation between the crystal symmetry, electronic structure and magnetic order of Pd. We have shown that for Pd in the fcc structure a magnetic moment occurs only at the lattice expansion of 10% [see Fig. 19(b)], saturating at the lattice expansion of 32%, where it attains the value of $0.36\mu_B$ [see Figs. 19(a) and 19(b)]. The magnetic moment of both hcp and *d*hcp Pd attains the same saturation value,[85] but at smaller lattice expansion [Fig. 19(b)]. As a result, residual magnetic moments of $0.11\mu_B$ and $0.16\mu_B$ for *d*hcp and hcp Pd, respectively, remain at the equilibrium lattice constants.

Now, an explanation of the occurrence (or nonoccurrence) of ferromagnetic order in various crystal structures of Pd can be provided by the calculated density of states (Fig. 19). The DOS of bcc Pd of $N(E_F)=1.1$ at the Fermi level [Fig. 19(d)] is too small to satisfy the Stoner criterion for ferromagnetism. Even lattice expansion would not increase it sufficiently to fulfill this criterion. In contrast, fcc Pd has, even at the optimum lattice constant, the density of states at the Fermi level of $N(E_F)=2.30$ [Fig. 19(d)], which is more than 2 times higher than in the previous case. Unfortunately, as it is seen in Fig. 19(b) it is not high enough to induce a ferromagnetic spin alignment in the structure. Consequently, ferromagnetism can only be induced in fcc Pd by lattice expansion [Fig. 19(b)]. Figures 19(e) and 19(f) show that Pd in the hexagonal close-packed structure has the density of states at the Fermi level of $N(E_F)=2.60$ for hcp Pd and of $N(E_F)=2.50$ for *d*hcp Pd. The DOS of hcp Pd and *d*hcp Pd is also increased in the immediate vicinity of the Fermi level in comparison to fcc Pd. Thus, our calculation shows that, as expected, fcc Pd is nonmagnetic, but hcp and *d*hcp Pd are ferromagnetically ordered at the optimum lattice constants. According to a recent itinerant theory of magnetism[86] a ferromagnetic state is stabilized at low enough temperatures, if an almost dispersionless band exists within broad ones. We will now identify in the band structures of hcp and *d*hcp Pd

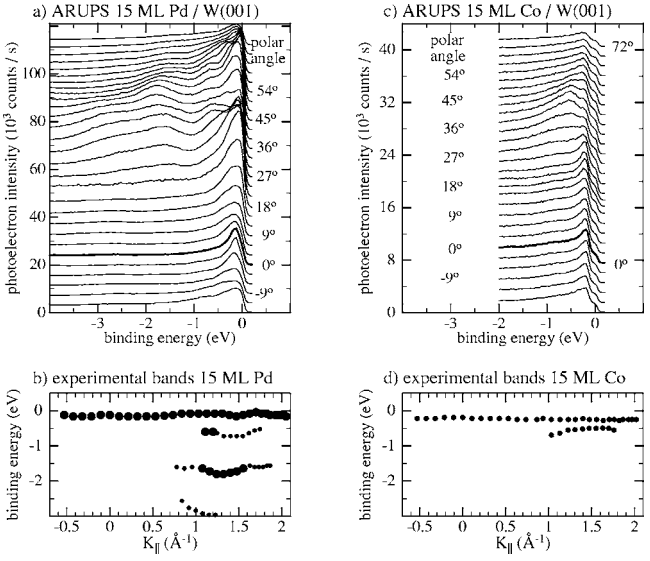

FIG. 20. (a), (c) ARUPS taken from a 15 ML thick $(11\bar{2}0)$-oriented Pd [panel (a)] and Co (c) film grown on W(001). The emission angle Θ was changed in the high symmetry [0001] and $[1\bar{1}00]$ directions [which are parallel to the $[110]_W$ direction of the W(001) surface]. The polar angle was changed from −15 to 72 degrees in steps of 3 degrees. The data were collected at 150 K. (b), (d) $E(k_\parallel)$ dependence for a 15 ML thick $(11\bar{2}0)$-oriented Pd (b) and Co (d) film in the [0001] and $[1\bar{1}00]$ directions determined from the ARUPS spectra of panels (a) and (c), respectively. In panel (b) large (small) circles correspond to strong (weak) UPS peaks.

dispersionless bands which lead to the density of states at the Fermi level high enough to induce ferromagnetism in these structures. The identification of these Pd bands which are flat at the Fermi level will be done through a comparison of the experimentally obtained band structure of *d*hcp (hcp) Pd films with the corresponding calculated bands of fcc, hcp, and *d*hcp Pd.

But before that, let us note the interesting sharp and strong peak in the DOS of bcc Pd situated at −0.7 eV [Fig. 19(c)]. This peak is much stronger than the other peaks and also higher than the peaks of the fcc, hcp, and *d*hcp DOS [Figs. 19(c), 19(d), 19(e), and 19(f)]. If a metal had the Fermi level there, a preferential spin alignment would very probably be established in that metal. Obviously, such a metal would have to have the bcc crystal structure and a *d*-band occupancy with one or a little more than one electron smaller than that of Pd. According to our calculation, Rh, which is also nonferromagnetic in its natural fcc crystal structure, has the Fermi level positioned exactly in the sharp strong peak of the bcc phase. Consequently, bcc Rh is ferromagnetically ordered with the magnetic moment of $0.26\mu_B$ at the equilibrium lattice constant.[87]

3. ARUPS from hcp Pd films in comparison to UPS from Co and Ni films

Pd on W(001) (Ref. 33) shows the same crystal structure and the same single, strong peak close to the Fermi level as Pd bonded to Nb(001). Figure 20(a) displays ARUPS spectra measured at different emission angles in a 15 ML thick, hexagonal close-packed (hcp, *d*hcp) Pd film grown on W(001).

The emission angle (θ) was changed along the $[110]_W$ direction of the W(001) surface. Taking into account the epitaxial relations of Pd on W(001) and the fact that ARUPS averages over the investigated part of the sample, the measured $E(k_\parallel)$ is a lateral average over the $[0001]_{Pd}$ and $[1\bar{1}00]_{Pd}$ directions. The resulting $E(k_\parallel)$ dependence[55] of the 15 ML thick Pd film is presented in Fig. 20(b). It shows the sought for flat band lying very close to the Fermi level (at the binding energy of less than −0.2 eV). Exactly such a flat band is obtained for Co films deposited on W(001) [see Figs. 20(c) and 20(d)]. The reason for this similarity lies in the same crystal structure orientation and band split caused by ferromagnetic order. Co on W(001) and Pd on W(001) or Nb(001) both grow in the $(11\bar{2}0)$-oriented hcp structure. A $(11\bar{2}0)$-oriented bulk sample of Co also shows in UPS only an emission near the Fermi energy.[58–60] Similarly, a strong UPS emission at the Fermi edge is characteristic of $(11\bar{2}0)$-oriented Ni films.[56,77] It should be pointed out, however, that the same crystal structure does not necessarily lead to the same UPS emissions. For example, $(11\bar{2}0)$-oriented Au films show different UPS emissions than these discussed here.[42] The reason why UPS emissions from $(11\bar{2}0)$-oriented Pd, Co, and Ni films are pretty much the same lies in their originating in one part of the band structure, which has a similar energy position for the three metals. Due to the ferromagnetic band split,[88] the majority bands of Co, Ni and even those of hcp Pd are almost completely filled, and as a result, have the same energy positions. Since band dispersion is determined by crystal symmetry, the same crystallographic structure, orientation and the ferromagnetic band split result in UPS emissions from $(11\bar{2}0)$-oriented Co, Ni, and Pd which are similar.

4. Comparison of the experimental bands of hcp Pd films with the calculated bands of fcc, hcp, and dhcp Pd

Comparing the measured flat Co band lying close to the Fermi level [Fig. 20(d)] with the bands calculated in the framework of DFT, we were able to identify it as one of the spin-majority bands in the band structure of hcp Co. We will now check whether a similar $E(k_\parallel)$ band exists in the band structures of fcc, hcp or *d*hcp Pd. However, to draw these bands we need to know the values of $k_\perp$.

Unfortunately, the refraction of photoelectrons on an unknown surface barrier potential leaves the $k_\perp$ component of a wave vectors unknown.[55] It can still be determined from a comparison of ARUPS measurements using more photon energies (e.g., using synchrotron radiation) with the relevant bulk band structure. This is possible since the energy position of a peak in ARUPS originating from a bulk state shifts as a function of the photon energy if the bulk band (from which the emission occurs) has energy dispersion. Such shifts in ARUPS as a function of the photon energy at a fixed parallel component of the wave vector are characteristic of direct transitions between bulk electronic states and have been observed in substrates like Nb(001).[89] Although the

electronic structure of confined ultrathin metallic films can also be fully explained in terms of the bulk band structure,[42,90,91] a variation of the photon energy does not necessarily lead to a shift of the energy positions of ARUPS peaks. Also in the case of thick metallic films, where the bulk behavior of ARUPS peaks is expected, such shifts may not necessarily occur.[90,91] Thus a determination of the normal component of a wave vector using synchrotron radiation does not need to be successful in the case of our ultrathin Pd films.

The aim of the following analysis is not to determine the normal components of the wave vectors but only to compare the measured flat $E(k_\parallel)$ bands with the bulk band structures, in order to identify in the latter ones flat $E(k_\parallel)$ bands situated close to the Fermi level. Since we do not know the value of $k_\perp$ of the emitting state we will compare the measured $E(k_\parallel)$ dependence of the band lying just below the Fermi level [as in Fig. 20(b)] with the calculated $E(k_\parallel)$ dependence for all the states of the fcc, hcp, and *d*hcp Pd band structures which have the binding energies of approximately −0.20 eV at $k_\parallel = 0$. Taking into account that the fcc(110) orientation has the best fit to the W(001) and Nb(001) surfaces from all the fcc orientations,[77] we will compare bands of the hcp and *d*hcp structures in the $(11\bar{2}0)$ direction with those of the fcc structure in the (110) direction. This means that $k_\perp$ and $k_\parallel$ will be parallel to [110] and (110) planes, respectively.

Figures 22(a)–22(c) show the bands of fcc, hcp, and *d*hcp Pd, respectively, in the direction normal to the surface of the films which is [110] for the fcc and $[11\bar{2}0]$ for the hcp and *d*hcp structures, respectively. These $E(k_\perp)$ bands correspond to $k_\parallel = 0$ and are not symmetric with respect to the Brillouin zone boundaries situated at points *K*, but with respect to point $k_\perp = \pi/d$, where $d = a/2$ is the distance between two adjacent (110) planes and $a = 2.75$ Å is the nearest-neighbor distance in fcc Pd. Point $k_\perp = \pi/d$ has inversion symmetry and is marked by *X* for the fcc structure and by *M* for the hcp and *d*hcp structures. These points lie exactly between two Γ points in the [110] direction of the Brillouin zone. The $E(k_\perp)$ bands show similar dispersions, except when $k_\perp$ reaches point *K*, i.e., the Brillouin zone boundary. Unlike in the fcc Brillouin zone, point *K* is in the hexagonal Brillouin zone a point of symmetry.[92] This leads to flatter dispersion of the hcp and dhcp bands around it, which is a crystal symmetry effect. Perpendicularly to the surface, there lie the hexagonal densest layers which are identical for the hcp, *d*hcp (0001) and fcc structure (111). The stacking sequence axes ([0001], [111]), which give the different stacking sequence of the hexagonal densest planes, lie in the surface plane. So, it is to be expected, that the band structures of hcp, *d*hcp, and fcc differ much more in that plane. Since the (110) surface of our films, being the $k_\parallel$ plane, contains the stacking sequence axis, the $E(k_\parallel)$ bands should be more affected by a different stacking sequence than the $E(k_\perp)$ bands discussed above.

Figure 21 depicts the periodicity of the hexagonal (hcp, *d*hcp) [panels (a), (b), (c)] and cubic (fcc) [panels (d), (e), (f)] structure in the reciprocal space (*k* space) and Fig. 22 depicts the bulk band structure of fcc, hcp, and *d*hcp Pd in the $k_\perp$ direction at $k_\parallel = 0$. In the case of fcc Pd there are four bands which contain states at $E_B \sim -0.20$ eV and $k_\parallel = 0$ [Fig. 22(a)]. The respective $k_\perp$ values for these states in units of $\pi/(40d)$ are 13, 29, 37, and 38. The corresponding $E(k_\parallel)$ bands to which these states belong are given in Fig. 23(a).

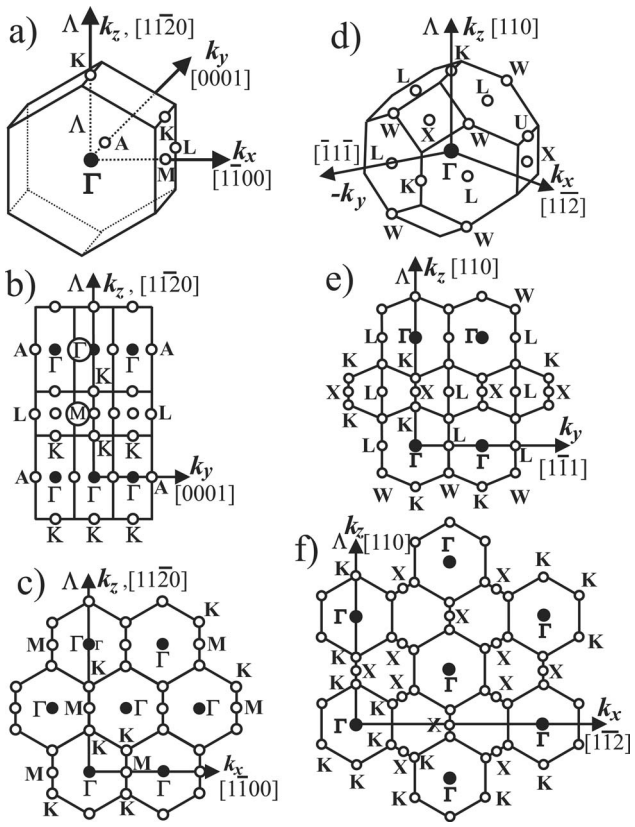

FIG. 21. (a), (d) Hexagonal [panel (a)] and fcc (d) bulk BZ. (b), (c) Hexagonal BZ in the repeated zone scheme in the $(k_y = 0)$ plane [panel (b)] and in the $(k_x = 0)$ plane [panel (c)]. (e), (f) fcc BZ in the repeated zone scheme in the $(k_y = 0)$ plane (e) and in the $(k_x = 0)$ plane (f). Axes k_x, k_y, k_z of the Cartesian coordinate system shown in panel (a) are parallel to the $[1\bar{1}00]$, [0001], $[11\bar{2}0]$ directions, respectively. $k_\perp$ is parallel to $[11\bar{2}0]$ and $k_\parallel$ lies in the k_{xy} plane. Axes k_x, k_y, k_z in panel (d) are parallel to the [211], [111], [110] directions, respectively. Here $k_\perp$ is again directed along [110] and the $k_\parallel$ plane is parallel to the k_{xy} plane. Points Γ are marked with black filled circles. The scale of (b), (c) and (e), (f) is two times smaller than that of (a) and (d), respectively.

None of them, however, has the flatness of the experimental band shown in [Fig. 20(b)].

Figures 23(b)–23(f) show the $E(k_\parallel)$ dependence in the high symmetry directions [0001] and $[1\bar{1}00]$ for the hcp and *d*hcp states whose energy at $k_\parallel = 0$ is $E_B \sim -0.20$ eV. For hcp Pd the state with $E_B \sim -0.20$ eV at $k_\perp = \pi/(2d)$ and $k_\parallel = 0$ (marked with circles) is almost dispersionless in the $[1\bar{1}00]$ direction, having the energy dispersion of less than 0.20 eV. Similarly, the state with $k_\perp = 3\pi/(4d)$ (marked again with circles) is almost dispersionless in the [0001] direction. In general, the Pd states in the hcp structure exhibit less $E(k_\parallel)$ dispersion than the Pd states in the fcc crystal structure. It follows from Figs. 23(d)–23(f) that the Pd states in the *d*hcp crystal phase modification, especially the states in the stacking sequence direction ([0001]), show even less energy dis-

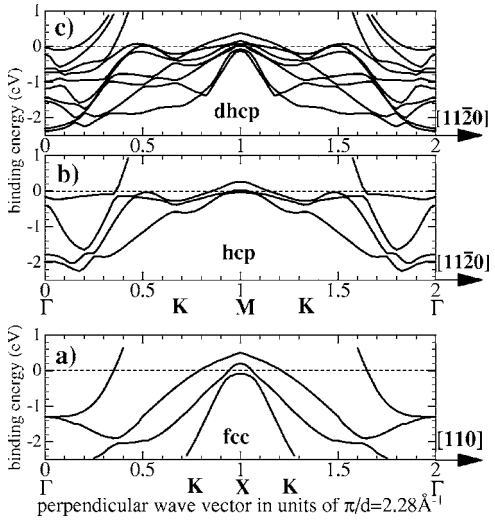

FIG. 22. Bulk band structure $[E(k_\perp)]$ of fcc (a), hcp (b), and *d*hcp (c) Pd in the [110] and [11$\bar{2}$0] directions, respectively.

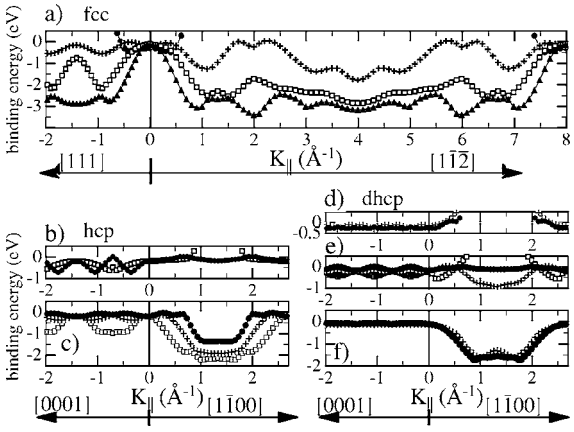

FIG. 23. $E(k_\parallel)$ bands of fcc (a), hcp (b), (c) and *d*hcp Pd (d), (e), (f) obtained in non-spin-polarized DFT calculations with spin-orbit coupling included (to be compared with the experimentally determined $E(k_\parallel)$ bands [Fig. 20(b)]). (a) Dispersion in the [111] and [1$\bar{1}$2] directions of the fcc Pd states which at $k_\parallel=0$ have, according to Fig. 22(a), $E\sim 0.20$ eV and $k_\perp=(13/40)\pi/d$ (circles), $k_\perp=(29/40)\pi/d$ (crosses), $k_\perp=(37/40)\pi/d$ (squares), and $k_\perp=(38/40)\pi/d$ (triangles). (b) Dispersion of the hcp-Pd states with $k_\perp=(5/40)\pi/d$ (squares), $k_\perp=(20/40)\pi/d$ (circles). (c) Dispersion of the hcp states with $k_\perp=(30/40)\pi/d$ (circles), $k_\perp=(33/40)\pi/d$ (crosses), and $k_\perp=(35/40)\pi/d$ (squares). (d) Dispersion of the *d*hcp Pd states with $k_\perp=(8/40)\pi/d$ (crosses), and $k_\perp=(13/40)\pi/d$ (circles). (e) Dispersion of the *d*hcp states with $k_\perp=(17/40)\pi/d$ (circles), $k_\perp=(29/40)\pi/d$ (crosses), and $k_\perp=0$ (squares). (f) Dispersion of the *d*hcp states with $k_\perp=(35/40)\pi/d$ (circles), $k_\perp=(37/40)\pi/d$ (crosses). For the $k_\parallel$ periodicity of the plotted fcc, hcp, and *d*hcp states see Fig. 21.

persion than those in the hcp phase. Thus the $E(k_\parallel)$ dependence discussed above clearly shows that the reduction of symmetry from fcc to hcp and *d*hcp leads to bands characterized by less energy dispersion, especially in the stacking-sequence directions, in which the Brillouin zone becomes smaller. The flatness of the bands results in an increased DOS at the Fermi level, which becomes large enough to induce ferromagnetism in *d*hcp and hcp Pd even at the optimum lattice constant.

5. Nonmagnetic ARUPS measurements—indication of ferromagnetic order in hcp Pd

The energy bands of ferromagnetically ordered hcp and *d*hcp Pd are split by 0.16 eV and 0.11 eV, respectively. Thus, the minority and majority bands should be discernible in state of the art photoemission experiments. Although our ARUPS measurements are unfortunately nonmagnetic, they show indications of band splitting. Both normal emission Ne I or He I UPS spectra taken with higher energy resolution (through the reduction of the pass energy of the analyzer) show that the peak close to the Fermi level is composed of peaks situated at some −0.41 eV, −0.25 eV, and −0.09 eV [Fig. 24(a)]. They are separated just by 0.16 eV, in accordance with the band splitting predicted for hcp Pd.

Unfortunately, an increase of the energy resolution of our UPS experiments is accompanied by a reduction of the emitted signal with respect to the background one. Thus, in UPS measurements a certain balance between the energy resolution of the analyzer and the strength of the emitted signal in comparison to the background one must be established. In our laboratory setup we use the pass energy of 2 eV which gives the energy resolution of 60 meV. With this pass energy the peaks of Fig. 24(a) are more difficult to be resolved because they are energetically very close to each other, and effectively merge into one broad peak. A further evidence

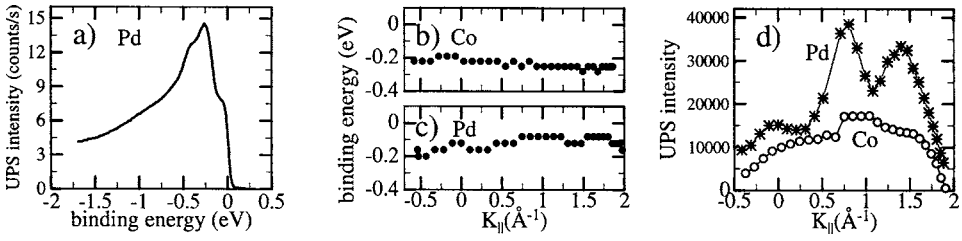

FIG. 24. (a) Normal emission Ne I-UPS from a 16 ML thick (11$\bar{2}$0)-oriented Pd film grown on Nb(001) taken with increased energy resolution (pass energy of 1.2 eV instead of 2 eV). (b), (c) The $E(k_\parallel)$ dependence of a 12 ML thick (11$\bar{2}$0)-oriented Co film (b) and of a 15 ML thick (11$\bar{2}$0)-oriented Pd film (c) grown on W(001) in the [0001] and [1$\bar{1}$00] directions. (d) UPS-rocking curves, the dependence of the intensity of the UPS peak close to the Fermi level on the emission angle (and, therefore, also on $k_\parallel$) for hcp Pd (marked with stars) and hcp Co (marked with circles) in the [0001] and [1$\bar{1}$00] directions.

whether the peaks of Fig. 24(a) are caused by ferromagnetic order can be furnished by the observation of the splits in the UPS intensity over the entire $k_{\|}$ region. If one of the bands (a minority band) crossed the Fermi level, it would lead to a drop in the UPS emission (UPS emission comes only from occupied states). If in addition a majority band is situated closer to the Fermi level than the value of the band split, the minority band would be unoccupied making photoemission from it impossible. We have observed exactly such a behavior and the respective curves are shown in Fig. 24. The curve marked with stars in Fig. 24(d) shows the UPS intensity of the strong peak positioned close to the Fermi level in Fig. 20(a) as a function of $k_{\|}$, which was calculated from the emission angles. As mentioned previously (Sec. III B 3), similar ARUPS emissions (i.e., a single, strong peak close to the Fermi level) were obtained from $(11\bar{2}0)$-oriented, ferromagnetically ordered hcp Ni (Refs. 56 and 77) and hcp Co.[33,57–60] The UPS intensity curve related to the flat $E(k_{\|})$ band situated close to the Fermi level of $(11\bar{2}0)$-oriented hcp Co films grown on W(001) [Fig. 24(b)] is marked with circles in Fig. 24(d). It shows a broad peak centered at some $k_{\|}=1$ Å^{-1}. The results of Matzdorf *et al.*[93] as well as our UPS-rocking curves obtained from various films [like (111)-, (001)- and (110)-oriented Au films) and single crystals, show that the intensity variation of ARUPS emissions from flat bands is caused by the diffraction of photoelectrons inside the crystal on their way toward the surface. The Pd-UPS rocking curve, marked with stars in Fig. 24(d), has been obtained using photoelectrons of the same kinetic energy and diffracted by the same crystal structure as those used for the Co-UPS rocking curve [circles in Fig. 24(d)]. Thus, it can be expected, that the Pd-UPS rocking curve show a similar broad peak centered at $k_{\|}=1$Å^{-1}. However, the curve in Fig. 24(d) shows a sudden drop in the intensity at around 1 Å^{-1}. We further argue that it comes from a band split caused by the ferromagnetic order. As it is shown in Fig. 24(c), the band disperses slightly from $k_{\|}=0.15$ Å^{-1} to $k_{\|}=0.75$ Å^{-1}, with the respective band energy changing from ~ -0.2 eV to ~ -0.09 eV. If the hcp-Pd bands are split by ~ 0.16 eV (or ~ 0.11 eV), then in the range 0.8 Å^{-1} to 1.25 Å^{-1} the minority band is unoccupied. Consequently, the strong UPS-peak close to the Fermi level should lose at $k_{\|}=0.8$ Å^{-1} the contribution of the emission from the minority band, and, as a result, the UPS emission should decrease. This is confirmed by the Pd-UPS intensity in Fig. 24(d). In the case of the UPS rocking curve for hcp Co a similar drop does not occur, because the band split is larger than 1 eV, which means, that the UPS emission from Co observed at −0.2 eV comes only from a minority or only from a majority band. It is worth mentioning here that the recent measurements of Sampedro *et al.*[94] on Pd particles show that Pd atoms lying in a stacking fault (i.e., in an hcp or *d*hcp environment) are ferromagnetically ordered.

IV. CONCLUSION

Our experimental and theoretical results show that the bonding of Pd to Nb(001) can induce noble-metal properties in a Pd ML bonded directly to Nb(001) and ferromagnetic order in thicker Pd films. The bonding of the Pd ML to Nb(001) shifts the density of states of the Pd ML to lower binding energies, similar to those of the noble-metal Cu, which results in a surface having noble-metal properties. Submonolayer Pd coverages on Nb(001) or Pd incorporated in the bulk of the Nb(001) substrate have even more Pd states shifted to lower binding energies. In contrast, thick Pd films deposited on Nb(001) show a strong UPS peak just below the Fermi level. Responsible for this is the quadratic arrangement of the Nb(001) surface which stabilizes via epitaxial constraint a hexagonal close-packed (hcp, *d*hcp) stacking sequence of Pd in films thicker than 100 ML. Relativistic self-consistent DFT calculations with spin-orbit coupling included show that the change of crystal symmetry from fcc to hcp and *d*hcp induces ferromagnetism in bulk Pd at the optimum lattice constant, with the magnetic moment of $0.11\mu_B$ per atom for *d*hcp Pd and of $0.16\mu_B$ for hcp Pd. This is caused by an increase of the DOS at the Fermi level large enough to satisfy the Stoner criterion for ferromagnetism. This increase can be attributed to the occurrence of flat bands at the Fermi level only in the band structure of hcp (*d*hcp) Pd. We identified such flat bands lying close to the Fermi level in hcp (*d*hcp) Pd films grown on Nb(001) using nonmagnetic photoelectron spectroscopy.

*Corresponding author. Electronic address: osuchk@science.unisa.ac.za

[1] B. E. Nieuwenhuys, Adv. Catal. **44**, 259 (2000).
[2] E. C. Stoner, Proc. R. Soc. London, Ser. A **165**, 372 (1938); **169**, 339 (1939).
[3] S. Blügel, Phys. Rev. Lett. **68**, 851 (1992).
[4] L. Fritsche, J. Noffke, and H. Eckardt, J. Phys. F: Met. Phys. **17**, 943 (1987).
[5] G. A. Prinz, Science **282**, 1660 (1998).
[6] Various contributions in *Handbook of Ferromagnetic Materials*, edited by K. H. J. Buschow (Elsevier, Amsterdam, 1993), Vol. 7.
[7] Various contributions in *Ultrathin Magnetic Structures I*, edited by J. A. C. Bland and B. Heinrich (Springer, Berlin, 1994); in *Ultrathin Magnetic Structures II*, edited by J. A. C. Bland and B. Heinrich (Springer, Berlin, 1994).
[8] Various contributions in *Science and Technology of Nanostructured Magnetic Materials*, edited by G. C. Hadjipanayis and G. A. Prinz (Plenum, New York/London, 1990), NATO ASI Series B, Vol. 259.
[9] H. Dreyssé and C. Demangeat, Surf. Sci. Rep. **28**, 65 (1997), and references therein.
[10] K. Heinz, S. Müller, and L. Hammer, J. Phys.: Condens. Matter **11**, 9437 (1999); and various other contributions in this special issue [J. Phys.: Condens. Matter **11** (48), 1 (1999)], Magnetism at surfaces, interfaces, and thin films containing invited papers on surface magnetism.
[11] K. Heinz, J. Phys.: Condens. Matter **15**, S655 (2003).
[12] D. Sander, J. Phys.: Condens. Matter **16**, R603 (2004).

[13] Various contributions in *Magnetic Surfaces, Thin Films, and Multilayers*, edited by S. P. Parkin, H. Hopster, J.-P. Renard, T. Shinjo, and W. Zinn (Materials Research Society, Pittsburgh, 1992), Vol. 231.

[14] N. R. Gall', E. V. Rut'kov, and A. Y. Tontegode, JETP Lett. **79**, 218 (2004), and references therein.

[15] Fullerenes are pure carbon molecules (e.g., C_{60} molecules) with a spherical form, which are considered as a highly promising material for nanoelectronics with a very diversified application field ranging from medicines to the components of nuclear explosive devices (Ref. 14). The use of fullerenes in virtually any sort of physical technology entails their interaction with solid surfaces. It was shown recently that a sulfur monolayer passivates the Ta(001) surface to such an extent that it protects the fullerene molecules against a catalytic action of the metal surface (Ref. 14). During thermal treatment, the fullerenes desorb from a sulfur passivated Ta(001) surface without decomposing and hence without contaminating the surface with carbon. The disadvantage of the sulfur terminated Ta(001) surface lies in the fact that fullerenes do not wet this surface (i.e., they form three-dimensional islands directly on the surface without first forming an intermediate adsorbate layer). This can be changed when fullerenes are deposited on a metallic or semiconductor surface (Ref. 14). However, the metallic and semiconductor surfaces used thus far have the disadvantage of bonding, through catalytic action, the first fullerene ML so strongly that the fullerene molecules cannot desorb without fragmentation and contamination of the surface and the bulk of a metal or semiconductor sample. Now, the ps Pd ML on Nb(001) can provide the both desired properties, its metallic character will very probably lead to a layer-by-layer growth of the deposited fullerenes and its nobleness will successfully prevent the decomposition of fullerenes making their complete removal from the surface possible, without contaminating the sample with carbon.

[16] A pseudomorphic ML is an ML which adopt (possess) the lateral lattice of the substrate surface.

[17] G. A. Landrum and R. Dronskowski, Angew. Chem., Int. Ed. **38**, 1389 (1999); **39**, 1560 (2000); R. Dronskowski, Int. J. Quantum Chem. **96**, 89 (2004).

[18] B. Frick and K. Jacobi, Phys. Rev. B **37**, 4408 (1988); B. Frick and K. Jacobi, Surf. Sci. **178**, 917 (1986); B. Frick, K. Jacobi, J. A. Wilder, H. J. Sagner, and K. H. Frank, *ibid.* **193**, 529 (1988); J. Colbert, A. Zangwill, M. Strongin, and S. Krummacher, Phys. Rev. B **27**, 1378 (1983); O. Rader, C. Carbone, W. Clemens, E. Vescovo, S. Blügel, W. Eberhardt, and W. Gudat, *ibid.* **45**, 13823 (1992); G. W. Graham, Surf. Sci. Lett. **171**, L432 (1986); G. C. Smith, C. Norris, C. Binns, and H. A. Padmore, J. Phys. C **15**, 6481 (1982); O. Bisi and C. Calandra, Surf. Sci. **67**, 416 (1977).

[19] F. Jona and P. M. Marcus, Surf. Rev. Lett. **4**, 817 (1997).

[20] There exist a number of experimental (Refs. 21–26) and theoretical (Refs. 25–29) reports on Pd bonded on the dense-packed (110) surface of Nb (Refs. 21, 22, 25, and 27) or Ta (Refs. 23, 24, 26, 28, and 29), showing that Pd electronic states lie at deep energies, like those of Cu. However, there are no studies, either theoretical or experimental, of the electronic structure of a Pd ML bonded to the much more open (001) surface of Nb or Ta. The evaluation of the bond strength between Pd and Nb(100) (Refs. 26, 31, and 32) has shown that it is stronger in (100)-oriented multilayers than in (110)-oriented superlattices. Thus, it is of interest to study the change occurring in the properties of a Pd ML when it is bonded to the (100) instead of (110) surface of Nb. In this work we will determine both experimentally and theoretically, the electronic structure of a ps (Ref. 16) monolayer of Pd bonded to a clean or sulfur terminated Nb(100). We will show that the strong bonds between Pd and Nb(100) lead to more Pd states lying at low energies than for Pd bonded to Nb(110), making Pd/Nb(100) more noble than Pd on Nb(110) or Ta(110).

[21] M. El-Batanouny, M. Strongin, G. P. Williams, and J. Colbert, Phys. Rev. Lett. **46**, 269 (1981).

[22] M. Sagurton, M. Strongin, F. Jona, and J. Colbert, Phys. Rev. B **28**, 4075 (1983).

[23] M. W. Ruckman, V. Murgai, and M. Strongin, Phys. Rev. B **34**, 6759 (1986).

[24] M. W. Ruckman and M. Strongin, Phys. Rev. B **35**, 487 (1987).

[25] M. El-Batanouny, D. R. Hamann, S. R. Chubb, and J. W. Davenport, Phys. Rev. B **27**, 2575 (1983).

[26] X. Pan, P. D. Johnson, M. Weinert, R. E. Watson, J. W. Davenport, G. W. Fernando, and S. L. Hulbert, Phys. Rev. B **38**, 7850 (1988).

[27] V. Kumar and K. H. Bennemann, Phys. Rev. B **28**, 3138 (1983).

[28] Š. Pick and P. Mikušík, J. Phys.: Condens. Matter **5**, 6581 (1993).

[29] R. Wu and A. J. Freeman, Phys. Rev. B **52**, 12419 (1995).

[30] Notice, Nb and Ta possess identical crystal structure and lattice constant. Furthermore, they have, in fact, also the same electronic valence structure expressed, e.g., by similar reactivities (Ref. 70). So, the bond of Pd to Nb(001) should be in fact very similar to that of Pd on Ta(001).

[31] M. Weinert, R. E. Watson, J. W. Davenport, and G. W. Fernando, Phys. Rev. B **39**, 12585 (1989).

[32] M. Weinert and R. E. Watson, Phys. Rev. B **51**, 17168 (1995).

[33] H. Wormeester, E. Hüger, and E. Bauer, Phys. Rev. B **54**, 17108 (1996).

[34] E. Hüger and K. Osuch, Europhys. Lett. **62**, 278 (2003).

[35] E. Bauer (private communication).

[36] L. Gmelin, R. J. Meyer, E. H. E. Pietsch, and E. Fluck, *Gmelin's Handbook of Inorganic and Organometallic Chemistry* (Verlag Chemie, Berlin, 1925), Vol. 49 B1.

[37] R. Franchy, T. U. Bartke, and P. Gassmann, Surf. Sci. **366**, 60 (1996).

[38] B.-S. Fang, C. A. Ballentine, and J. L. Erskine, Phys. Rev. B **36**, 7360 (1987); **38**, 4299 (1988); Surf. Sci. Lett. **204**, L713 (1988); B.-S. Fang, W. -S. Lo, and H. -H. Chen, Phys. Rev. B **47**, 10671 (1993); B.-S. Fang, W.-S. Lo, T. -S. Chien, T. C. Leung, C. Y. Lue, C. T. Chan, and K. M. Ho, *ibid.* **50**, 11093 (1994).

[39] P. Turban, L. Hennet, and S. Andrieu, Surf. Sci. **446**, 241 (2000)

[40] B. An, S. Fukuyama, K. Yokogawa, and M. Yoshimura, Phys. Rev. B **68**, 115423 (2003).

[41] E. Hüger, H. Wormeester, and K. Osuch, Surf. Sci. **580**, 173 (2005).

[42] E. Hüger and K. Osuch, Phys. Rev. B **68**, 205424 (2003).

[43] P. Hohenberg and W. Kohn, Phys. Rev. **136**, B864 (1964).

[44] W. Kohn and L. J. Sham, Phys. Rev. **140**, A1133 (1964).

[45] P. Blaha, K. Schwarz, G. K. H. Madsen, D. Kvasnicka, and J. Luitz, WIEN2K, *An Augmented Plane Wave + Local Orbitals Program for Calculating Crystal Properties* (Karlheinz Schwarz, Technical Universität Wien, Austria, 2001).

[46] R. Wu and A. J. Freeman, Phys. Rev. B **52**, 12419 (1995).

[47] M. van Schilfgaarde, V. P. Antropov, and B. N. Harmon, J. Appl. Phys. **79**, 4799 (1996).
[48] M. Körling and J. Häglund, Phys. Rev. B **45**, 13293 (1992).
[49] V. Ozolins and M. Körling, Phys. Rev. B **48**, R18304 (1993).
[50] It is well known that magnetic electronic structure calculations based on the LSDA approximation to the exchange-correlation potential predict a wrong ground state for Fe (fcc instead of bcc). This deficiency of the LSDA approximation has been remedied by the introduction of gradient corrections to the LDA. [For a list of references on this subject see Söderlind *et al.* (Refs. 51 and 52).]
[51] P. Söderlind, R. Ahuja, O. Eriksson, J. M. Wills, and B. Johansson, Phys. Rev. B **50**, 5918 (1994).
[52] P. Söderlind, J. A. Moriarty, and J. M. Wills, Phys. Rev. B **53**, 14063 (1996).
[53] The reason why the LSDA and not the more modern GGA approximation was used in this study is that the former gives better results for heavier elements whereas the latter is more suitable for lighter ones (Ref. 54). This is further confirmed by our spin-polarized, GGA calculation of the magnetic moment of Pd atoms in the fcc phase at the optimum lattice constant. It produces a nonvanishing magnetic moment, leading to the conclusion that fcc Pd is ferromagnetically ordered, in contradiction to experimental observations.
[54] P. Blaha (private communication).
[55] S. Hüfner, *Photoelectron Spectroscopy* (Springer, Berlin, 1995).
[56] N. B. Brookes, A. Clarke, and P. D. Johnson, Phys. Rev. B **46**, 237 (1992).
[57] W. Wulfhekel, T. Gutjahr-Löser, F. Zavaliche, D. Sander, and J. Kirschner, Phys. Rev. B **64**, 144422 (2001).
[58] B. Klingenberg, F. Grellner, D. Borgmann, and G. Wedler, Surf. Sci. **296**, 374 (1993).
[59] F. Grellner, B. Klingenberg, D. Borgmann, and G. Wedler, Surf. Sci. **312**, 143 (1994).
[60] F. Grellner, B. Klingenberg, D. Borgmann, and G. Wedler, J. Electron Spectrosc. Relat. Phenom. **71**, 107 (1995).
[61] M. El-Batanouny, M. Strongin, and G. P. Williams, Phys. Rev. B **27**, 4580 (1983), and references therein.
[62] F. J. Himpsel, J. E. Ortega, G. J. Mankey, and R. F. Willis, Adv. Phys. **47**, 511 (1998).
[63] J. A. Rodriguez and D. W. Goodman, Science **257**, 897 (1992); J. Phys. Chem. **95**, 4196 (1991); J. A. Rodriguez, Surf. Sci. Rep. **24**, 223 (1996).
[64] R. I. R. Blyth, P. T. Andrews, N. Heritage, and P. J. R. Birtwistle, J. Phys.: Condens. Matter **3**, 8869 (1991).
[65] J. C. Fuggle, F. U. Hillebrecht, R. Zeller, Z. Zołnierek, P. A. Bennett, and Ch. Freiburg, Phys. Rev. B **27**, 2145 (1983), and references therein.
[66] I. Turek, S. Blügel, and J. Kudrnovský, Phys. Rev. B **57**, R11065 (1998).
[67] P. E. A. Turchi, R. M. Waterstrat, R. Kuentzler, V. Drchal, and J. Kudrnovský, J. Phys.: Condens. Matter **16**, 5615 (2004).
[68] M. Tenhover and W. L. Johnson, Phys. Rev. B **27**, 1610 (1983).
[69] V. L. Moruzzi, P. Oelhafen, A. R. Williams, R. Lapka, H.-J. Güntherodt, and J. Kübler, Phys. Rev. B **27**, 2049 (1983).
[70] B. Hammer and J. K. Nørskov, Nature (London) **376**, 238 (1995); Surf. Sci. **343**, 211 (1995); B. Hammer, Y. Morikawa, and J. K. Nørskov, Phys. Rev. Lett. **76**, 2141 (1996); B. Hammer and J. K. Nørskov, in *Chemisorption and Reactivity on Supported Clusters and Thin Films*, edited by R. M. Lambert and G. Pacchioni (Kluwer Academic, Dordrecht/Boston/London, 1997), NATO ASI Series E: Applied Sciences, Vol. 331.
[71] J. K. Nørskov, J. Chem. Phys. **90**, 7461 (1989); K. W. Jacobsen, J. K. Nørskov, and M. J. Puska, Phys. Rev. B **35**, 7423 (1987).
[72] B. Hammer, Phys. Rev. Lett. **89**, 016102 (2002).
[73] H. Knoppe and E. Bauer, Z. Phys. Chem. (Munich) **202**, 45 (1997).
[74] D. R. Lloyd, C. M. Quinn, and N. V. Richardson, Surf. Sci. **63**, 174 (1977).
[75] Y. Kamada and M. Matsui, J. Phys. Soc. Jpn. **66**, 658 (1997).
[76] Z. Q. Wang, Y. S. Li, F. Jona, and P. M. Marcus, Solid State Commun. **61**, 623 (1987).
[77] E. Hueger, H. Wormeester, and E. Bauer, Surf. Sci. **438**, 185 (1999).
[78] S. A. Chambers, Adv. Phys. **40**, 357 (1991).
[79] D. P. Woodruff and A. M. Bradshaw, Rep. Prog. Phys. **57**, 1029 (1994); D. P. Woodruff, Surf. Sci. **299/300**, 183 (1994).
[80] W. F. Egelhoff, Jr., in *Ultrathin Magnetic Structures I*, edited by J. A. C. Bland and B. Heinrich (Springer, Berlin, 1994).
[81] Z.-L Han, S. Hardcastle, G. R. Harp, H. Li, X.-D. Wang, J. Zhang, and B. P. Tonner, Surf. Sci. **258**, 313 (1991).
[82] G. C. Gazzadi and S. Valeri, Europhys. Lett. **45**, 501 (1999).
[83] H. Wormeester, E. Hüger, and E. Bauer, Phys. Rev. Lett. **81**, 854 (1998).
[84] E. Hüger and K. Osuch, Europhys. Lett. **63**, 90 (2003).
[85] Our calculations show that the smaller magnetic moment of Pd in comparison to Ni can be attributed to the fact that Pd, and especially lattice expanded Pd, has many fewer *d*-band holes than Ni. The saturation limit of the magnetic moment of Pd is only reached after lattice expansion. During this process a shift from *sp*- to *d*-type occupancy occurs until Pd is atomiclike (i.e., has fully occupied *d* states). This leads to fewer states available for preferential spin alignment (spin down or spin up). The calculations also show that the spin-majority bands of Pd are fully occupied in the saturation limit. Thus, Pd, like Ni, should be a strong ferromagnet in this limit.
[86] F. J. Ohkawa, Phys. Rev. B **65**, 174424 (2002).
[87] E. Hüger and K. Osuch, Solid State Commun. **131**, 175 (2004).
[88] M. Černý, J. Pokluda, M. Šob, M. Friák, and P. Šandera, Phys. Rev. B **67**, 035116 (2003).
[89] B.-S. Fang, C. A. Ballentine, and J. L. Erskine, Phys. Rev. B **38**, 4299 (1988).
[90] T. -C. Chiang, Surf. Sci. Rep. **39**, 181 (2000).
[91] M. Milun, P. Pervan, and D. P. Woodruff, Rep. Prog. Phys. **65**, 99 (2002).
[92] C. J. Bradley and A. P. Cracknell, *The Mathematical Theory of Symmetry in Solids* (Clarendon, Oxford, 1972)
[93] R. Matzdorf, R. Paniago, G. Meister, A. Goldmann, and R. Courths, Surf. Sci. **343**, L1182 (1995).
[94] B. Sampedro, P. Crespo, A. Hernando, R. Litrán, J. C. Sánchez López, C. López Cartes, A. Fernandez, J. Ramírez, J. González Calbet, and M. Vallet, Phys. Rev. Lett. **91**, 237203 (2003).